9

Force Spectroscopy on Cells

9.1 Introduction 9-1
9.2 AFM and Force Spectroscopy 9-1
Manipulating the Nano-World (Angstrøms, Pico Newtons, and Molecular Handles) • Equilibrium Thermodynamics versus Forced Unbinding
9.3 Mechanical Properties of Single Molecules 9-6
Entropic Polymer Elasticity (the Worm-Like Chain Model) • Single Molecule Experiments
9.4 Force Spectroscopy on Living Cells 9-11
Cell Mechanics (Theory) • Molecular Concepts in Cell Adhesion • Cell Adhesion (Force Measurements)
9.5 Conclusions 9-25
9.6 Outlook 9-26
Acknowledgement 9-26
Abbreviations 9-26
References 9-26

Martin Benoit
Ludwig-Maximilians-Universität München

9.1 Introduction

In the human body, a vast variety of different molecules is circulating, diffusing, and interacting. Cell membranes contain many proteins that are responsible for interacting and communicating with their environment. Some examples are adhesion molecules for cell anchorage or locomotion, membrane pores for molecular exchange, and other receptor molecules. The receptor molecules specifically screen for information mediated by ligand-molecules (e.g., hormones) that match the binding site. Some cellular receptor molecules act like "noses," programmed to transduce the event of a bound ligand through the membrane into the cell by a conformational change (e.g., G-protein-coupled receptors). A change in conformation is a synonym for a mechanical deformation of the molecule. This often triggers a molecular reaction inside the cell by a signaling cascade. A few ligand molecules (e.g., chemokines) might change the behavior of the whole cell, for example, the directed motion along a concentration gradient. For cellular motion, reversible adhesion and force are required. In order to react adequately to external stimuli, a cell can utilize different concepts for tuning its adhesion by directly strengthening the adhesion of an adhesion molecule (affinity), by increasing the number of available adhesion molecules (avidity), or by altering the properties of the cellular anchor of the adhesion molecule. Additionally, the cell can distribute an external load to its adhesion molecules either in a sequential manner (pealing off from the adhesion site one bond after the other at low forces) or in parallel to the grouped adhesion molecules (clustered weak bonds that share the load in parallel and add it up to a very high force). To resolve the concepts behind cellular adhesion, techniques with a single molecular resolution as well as techniques that reveal multi-molecular arrangements are required. Force spectroscopy is a technique that measures forces within or between individual molecules. Performing such experiments on living cells at the level of single molecules not only reveals the strength of a molecular bond but also adhesion strategies and mechanical reactions of cells related to external forces. Like the receptor molecules, the adhesion molecules also scrutinize their environment for specific ligands, but they rather aim at mediating motility or anchorage of the cell. Some adhesion molecules also change their conformation if a ligand has bound and trigger molecular reactions inside the cell. With this concept, the cell can sense the mechanical and chemical properties of the environment it adheres to and consequently react to it. In the following chapter, the technique of force spectroscopy is applied to address questions about cell adhesion forces. How strong is the cell's adherence? What is the maximum force with which a cell can adhere? How does the cell regulate the adhesion strength? What force binds a single adhesion molecule to its ligand?

First, we detail the measurement of the cellular adhesion forces by using the atomic force microscope (AFM).

9.2 AFM and Force Spectroscopy

Like every scanning microscope, the AFM also consists of three basic units: a sensor (interacting with a surface very locally), a scanner (positioning either the probe or the sensor with respect to the sensor or the probe, respectively), and a detector (collecting

and converting the signal from the sensor). The force microscope is a mechanical instrument with a resolution to image atoms. Therefore, it is commonly called the atomic force microscope (Binnig et al., 1986). In contrast to the electron microscope (EM), the AFM can even operate in a liquid environment, gaining access to functional biomolecules and living cells. The central sensor of the instrument is a sharp tip on a cantilever that probes the sample mechanically. If the tip, mounted to a small beam that acts like a spring, experiences a force the beam is deflected.

In a small range, this deflection of the beam is proportional to the exerted force and is characterized by a spring constant k according to Hooke's law. A laser reflected from the backside of the cantilever spring reports the deflection Δz to a segmented photodetector with a sub-nanometer resolution. The force on the tip $\Delta F = k^{*}\Delta z$ can be detected at a few pico Newton resolution. In general, a piezo actuator positions and scans the sample in x–y–z direction at sub-nanometer accuracy. A typical setup of an AFM is shown in Figure 9.1.

The measured signal from the segmented photodetector coordinated with the three-dimensional position of the piezo yields a high-resolution image of the sample surface. Single molecules (Figure 9.3) and even single atoms are visualized with this technique (Hansma et al., 1988; Oesterhelt et al., 2000).

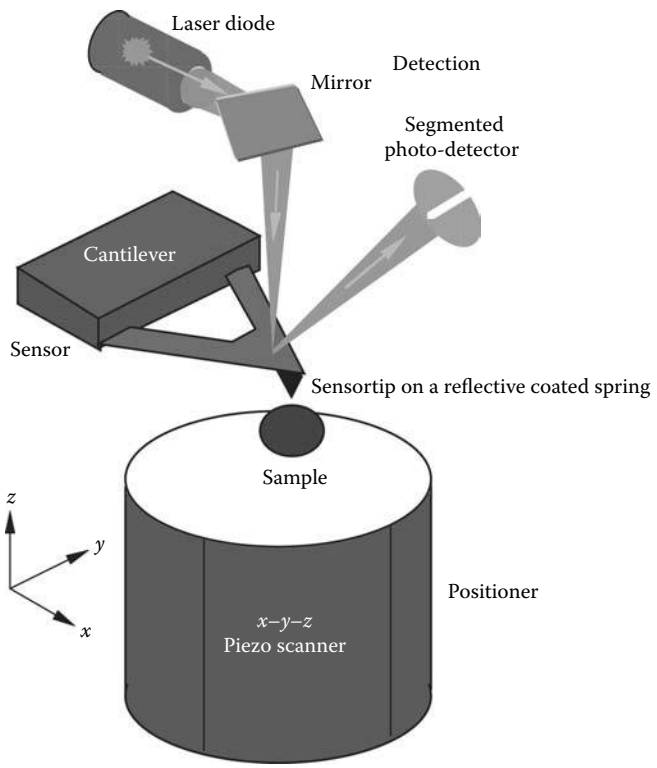

FIGURE 9.1 The AFM consists of three elements: The positioner, a voltage sensitive piezo crystal, coordinates the interaction of the sample and the cantilever tip with sub-nanometer precision. The force sensor is the micro fabricated cantilever with a small tip mounted to a reflective coated beam (here triangular). The movement of the reflected laser in the photo detector reports the deflection of this beam, due to forces acting on the tip.

For the improved force spectroscope designs, the scanning of the sample in the x–y direction is often disabled, in order to optimize the resolution in the z direction ($\Delta F = k^{*}\Delta z$). During the approach, in a typical force experiment, the repulsive force trace gives viscoelastic information about the sample. After a time of contact at a certain repulsive force, this force trace is reversed and even stretches the sample if adhesion occurs. Therefore, the sample has to be immobilized to the substrate. For receptor–ligand interaction measurements, spacer molecules are typically inserted into the system to avoid nonspecific interactions of the sample with the solid surfaces of the substrate and the tip (Figure 9.2). Such a nonspecific interaction is the first peak measured in the force graph of Figure 9.3 that was performed with a bare tip. Force spectroscopy experiments improve if molecular handles covalently link the spacer to a specific atom of the investigated molecule instead of "grabbing" the molecule nonspecifically with a bare tip. In the next examples of single molecule force experiments, both methods are utilized. The nonspecific method requires no tip functionalization, but the few "good force traces" have to be selected from the nonspecific. If the length of the molecule is known, a good selection criterion is the measured length of the molecule during the stretching calculated from an elastic model (see page 9-6).

9.2.1 Manipulating the Nano-World (Angstrøms, Pico Newtons, and Molecular Handles)

In the following example, the force spectroscopy is combined with high-resolution imaging of the AFM. A plain cantilever at high resolution imaged the bacteriorhodopsin (BR)—the light driven proton pump in the extracellular purple membrane of *Halobacterium salinaris*. BR consists of seven transmembrane alpha helices (helix "a" to "g" in Figure 9.3) forming a pore for protons. Three of these pores form a ring-like structure, as visualized in Figure 9.3. A nonspecific force spectroscopy experiment on this membrane led to the extraction of an individual BR molecule from this purple membrane and showed a typical unfolding pattern that perfectly correlates with the amino acid sequences of the pairs of alpha helices and their lengths.

Molecular handles cloned to the BR at specific amino acids in the loops between the helices or to the extracellular terminus of helix "a" provided certain access points of the molecule directly by a complementary receptor on the cantilever tip (Muller et al., 2002). However, the quality of an AFM image is reduced by such a functionalization of the cantilever. Here, we see two concepts of single molecule force experiments: nonspecific adhesion to a bare cantilever versus specific adhesion to a functionalized cantilever. Both concepts have complementary advantages and disadvantages.

The second concept, with defined spacer and specific handles, is highly reproducible and has an increased success rate. In particular, it has been validated for the generation of specific unfolding signatures of individual molecules (Carrion-Vazquez et al., 2000; Clausen-Schaumann et al., 2000; Rief et al., 2000a; Dietz and Rief, 2004). The use of linker molecules reduces the

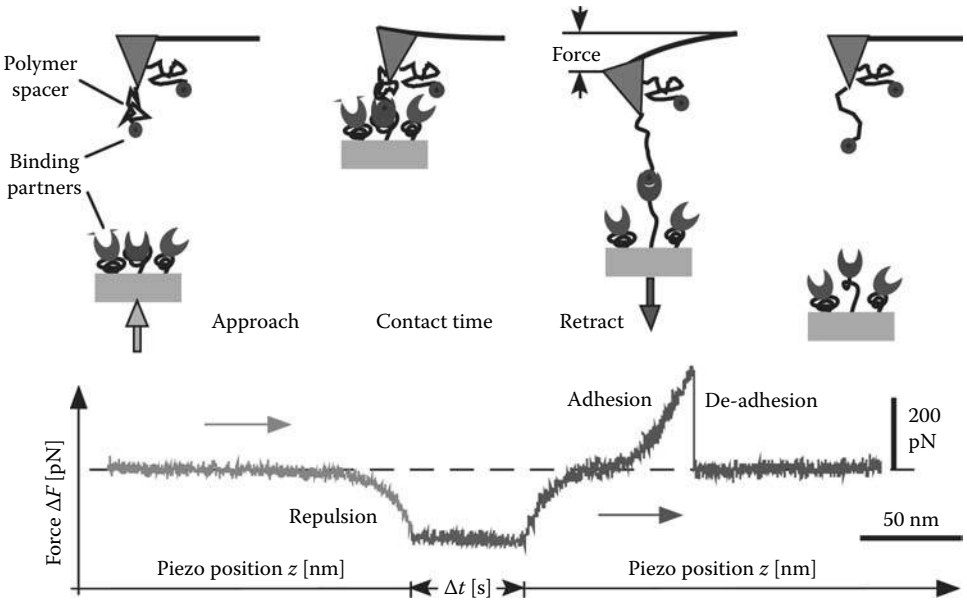

FIGURE 9.2 Sketch of single molecule force experiment with the recorded force trace below. The force sensor approaches at zero force until the repulsive interaction with the surface deflects the cantilever upward. This is represented by a negative repulsion force in the graph below. After a defined contact time the piezo motion is reversed and the repulsive force at the sensor tip is released. An adhesive interaction due to a receptor–ligand interaction deflects the force sensor downward. This is represented by the positive force characteristic for the spacer molecule (here PEG). Finally, the applied force overcomes the strength of the receptor ligand bond (here biotin–avidin) and the measured force drops instantaneously to zero.

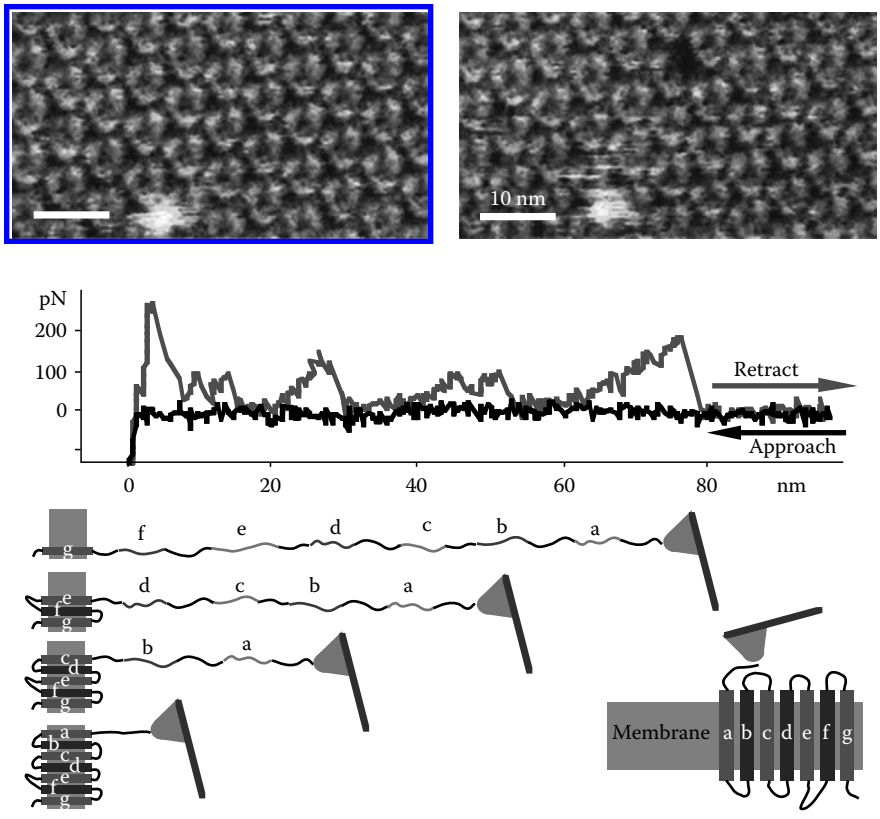

FIGURE 9.3 AFM images of individual bacteriorhodopsin molecules in a bacteria surface, before (left) and after (right) a single molecule force experiment. The peaks of the force curve between the two images are represented by the scheme below indicating (except the first peak from nonspecific interaction) the unfolding of alpha helices in pairs until the final extraction of helix "g" from the membrane. (From Oesterhelt, F. et al., *Science*, 288, 143, 2000. With permission.)

nonspecific interaction of the molecule with the surfaces (e.g., the bare cantilever tip).

The first concept is easy in preparation and has good imaging properties. To decide whether the measured force trace was specific or originated from some other nonspecific interaction, one hint is provided by the image lacking one molecule after the force experiment. Other hints are the characteristic force signature of the investigated molecule (should it be known already) and the constraints for the length of the molecule. According to this example, each experiment with a length that does not roughly match the amino acid length of the BR, indicates that a different molecule did attach to the tip (too long), or the BR molecule was "fished" somewhere else other than the terminus of the helix "a" (too short).

The use of polymeric molecular constructs that include an unknown molecule in the middle of a sequence of known molecules guarantees that the unknown force signature is included in the force trace if more than half of the known molecules were recognized in that force trace (Dietz and Rief, 2004; Kufer et al., 2005; Puchner et al., 2008b).

9.2.2 Equilibrium Thermodynamics versus Forced Unbinding

Viruses and bacteria developed molecules that specifically bind to the molecules on their target cell. In return, immune cells continuously screen the body for foreign molecules and produce antibodies that specifically bind to any molecule that does not belong to the organism. Pharmacology and pharmaceutical industry have characterized such receptor–ligand interactions for quite some time by their dissociation constant K_D to screen for more effective ligands, antibodies, or inhibitors with better K_D values, to develop better and more specific medication.

Force spectroscopy has opened up new avenues for measuring molecular interaction strengths. What is the mechanical force that holds an individual ligand in its receptor? In the illustration (Figure 9.4), this will be the force needed to pull the bond out of the potential valley of the binding energy, ΔG, and to lift it over the hill of the activation energy, ΔG_{on}. Theoretical work based on classical thermodynamics was offered by Bell (1978) and translated to force measurements by Evan (1998).

In thermodynamic equilibrium, we can measure the dissociation constant K_D of two substances a and b forming a complex ab. K_D is the fraction of the concentrations of the unbound ligands [a] and [b], and the complex [ab]:

$$K_D = \frac{[a][b]}{[ab]} = \frac{k_{off}^0}{k_{on}^0} \tag{9.1}$$

K_D also resembles the fraction of the kinetics k_{on} (how fast does a ligand bind at a given concentration?) and k_{off} (how fast is a ligand released?).

The binding energy is composed by

$$\Delta G = \Delta G_{off} - \Delta G_{on} \tag{9.2}$$

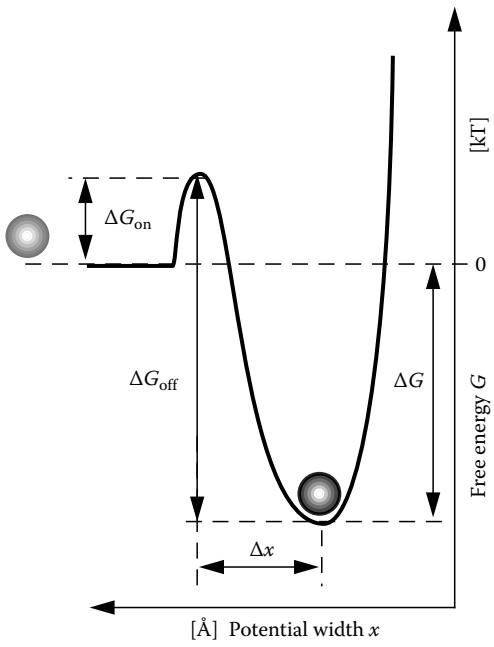

FIGURE 9.4 A symbolic receptor–ligand complex is represented by the sphere in the minimum of the potential valley. The energy barrier, ΔG_{off}, consisting of the Gibbs free energy, ΔG, and the activation energy, ΔG_{on}, has to be overcome to separate the receptor–ligand complex.

For 1 mol of molecules, the free energy without an external force is

$$\Delta G = \Delta H - T\Delta S = -N_A k_B T \ln K_D \tag{9.3}$$

k_B is the Boltzmann constant. Thus, for a single bond we can formulate

$$K_D = e^{-\frac{\Delta G}{k_B T}} \tag{9.4}$$

With force spectroscopy, we study the forces needed to separate the ligand from its receptor.

While the values gained from the thermodynamic equilibrium experiments do not change within a certain concentration limit, the unbinding force of a biotin–avidin bond, initially measured at 160 pN in 1996, turned out to range from 0 pN to more than 300 pN. Unfortunately, we will see that there is no "typical force" of a molecular bond but the force depends on the experimental setup and the history of the force application. A force sensor with a lower spring constant can measure lower forces. We will see that a bond generally opens at higher forces the lower the ambient temperature T is. An unbinding experiment done with faster separation velocities tends to result in higher forces than a slow experiment. What then is the sense in measuring such a force at all? It seems like a famous dilemma from quantum mechanics: The design of the experiment anticipates the result. The value of the wave function is created at the moment of measurement (particle or wave, momentum or location, moment

or energy). A key to this "dilemma of the force spectroscopy" is the thermal energy (Brownian motion) that randomly influences various packages of energy in the order of k_BT on every molecular bond.

9.2.2.1 Gedankenexperiment

If we consider an experiment without any external force, we will find a certain fraction (K_D) of molecules dissociated even without an external force! At higher temperatures, this fraction will be even bigger until the thermal energy (k_BT) far exceeds the energy of the molecular bond (ΔG) and almost no bond is stable anymore (Equation 9.4). Increasing the ambient temperature T in Figure 9.4 is like flooding the potential valley with thermal energy in a way that the complex "floats" on the increasing energy levels until it exceeds the energy barrier. This is the melting temperature of a molecular complex. In the absence of an external force, the fraction of dissociated bonds is solely generated by the stochastic impact of the thermal energy of the ambient temperature. If we apply a force at this temperature to that molecular bond, we support the thermal energy in dissociating the bond by adding mechanical energy and by rectifying the thermal motion of the complex: Once it is unbound, it stays unbound. If we apply the force very slowly, the probability for the bond to dissociate at forces close to zero due to the Brownian motion is still quite high. If we pull faster, we reduce the time to await the thermally driven unbinding. This results in a reduced unbinding probability and a reduced contribution to the bond dissociation of the thermal energy. Accordingly, the fraction of the additional required mechanical energy to overcome the potential barrier finally increases. As a consequence, we measure a statistically higher unbinding force according to the increasing remaining mechanical energy the faster we load the force to the bond. This behavior is represented by the concept of the loading rate (how fast is the force loaded to the bond?) as seen in Figure 9.5 (Merkel et al., 1999).

The Van't Hoff–Arrhenius equation under external force considers the separation of a single bond with a rate k_{off}:

$$k_{off} = \nu \cdot e^{-\frac{\Delta G_{off} - F\Delta x}{k_B T}} = k_{off}^0 \cdot e^{\frac{F\Delta x}{k_B T}} \tag{9.5}$$

where

- ν is a factor that can be viewed as a frequency that probes the potential landscape of the bond
- k_{off}^0 is the equilibrium off-rate in the absence of force

From this equation, we can see that the energy landscape depicted in Figure 9.11 becomes tilted by the subtraction of $F^*\Delta x$. The stronger the force, the more the potential is shifted. Deeper inner barriers become the maximum of the potential, the more the potential is shifted. The force experiment then probes the next potential valley behind the new highest barrier. After some calculations to be followed by literature (Walton et al., 2008), we come to the key equation for the most probable force F to be measured:

$$F(f) = \frac{k_B T}{\Delta x} \cdot \ln\left(f \cdot \frac{\Delta x}{k_{off} \cdot k_B T} \right) = \frac{\Delta G_{off}}{\Delta x} \cdot \ln\left(f \cdot \frac{\Delta x}{\nu \cdot k_B T} \right) \tag{9.6}$$

F logarithmically depends on the loading rate $f = dF/dt$. The Brownian motion affecting the bond results in a stochastic deviation around this force value. Thus, we call it the most probable rupture force. A well-conducted force spectroscopy experiment collects a statistically significant amount of

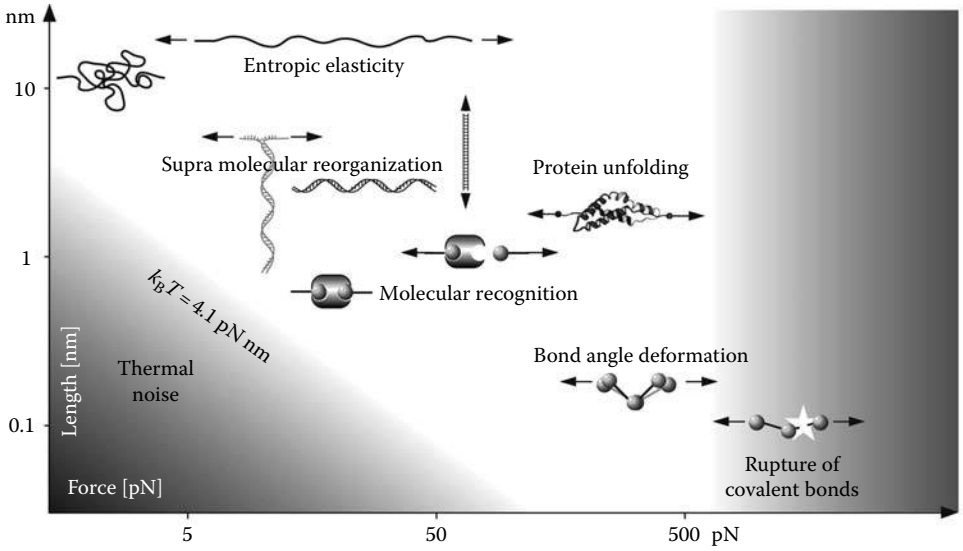

FIGURE 9.5 The potential width (Δx) versus force (F) graphic opens an energy window (white) for force measurements. Molecular bonds weaker than k_BT (located in the gray area below the diagonal line) are not stable at room temperature ($T = 293$ K). It is not possible to exert forces along a molecule that are stronger than the weakest covalent bond without disintegrating the molecule (gray area on the right hand side).

unbinding force measurements to determine this most probable unbinding force from the force distribution histogram (see Figure 9.12). From Equation 9.6, we can now understand the behavior of the forces in the overview graph of Figure 9.10: The most probable measured force increases with the logarithm of the loading rate and decreases with the temperature T (particularly since $\Delta G = \Delta H - T\Delta S$). Now we also understand that early MD-simulations on the biotin–avidin complex pulled with the velocities of nm/ps probed potentials that are far beyond the thermal energy range. Such deep potentials were probed force-spectroscopically by Michel Grandbois et al. for the first time in 1999 (Grandbois et al., 1999).

The AFM can be used for single molecule force experiments on biomolecules only in a window (Figure 9.5) between the force resolution limit of a few piconewton, a barrier of the thermal energy k_BT, and the strength of the weakest covalent bond in the spanned molecule chain. Below the AFM force resolution limit down to the Femto–Newton level, the optical and magnetic traps still can probe long ranged molecular interaction (Rief et al., 2000b; Kruithof et al., 2008). We know very well about that restriction due to the thermal energy, k_BT, at the experiments' temperature, since a complex with a binding energy $\Delta G \leq k_BT$ is statistically open and not stable enough to be probed by force spectroscopy.

9.2.2.2 Single Molecule Force Measurement versus Ensemble Measurement of K_D

From a mechanistic point of view, the thermal energy represented by the Brownian motion of the molecules steadily kicks against the complex from various directions and with various velocities and momentums. This stochastically forces the bond to open from time to time. With a force spectroscopic experiment, we only pull in one single direction. The slower we pull the more probable the thermal energy helps to open the bond. All these considerations are based on the Bell–Evans model (Bell, 1978; Evans, 1998). In a force spectroscopic experiment, we detect a single molecular force in cooperation with the thermal energy. We need statistically relevant numbers of single molecule measurements to identify the most probable unbinding force, and with the help of the Bell–Evans model, we can explore the potential landscape of the bond. The correlation to equilibrium thermodynamics with the help of the Jarzynski theorem (Collin et al., 2005) is sometimes complicated. The forces of many molecular interactions have been calculated back to the natural off-rates k_{off} measured by techniques such as calorimetry or SPR. Sometimes, the differences are still significant (Dettmann et al., 2000; Morfill et al., 2007) because force spectroscopy sets an unbinding direction that might not be used by equilibrium measurements, as we will see later (page 9-7). SPR and calorimetry also use theories, models, and parameters for their machines to recalculate the off-rate, the on-rate, and the dissociation constant, K_D, respectively. Another basic difference is that SPR and calorimetry do ensemble measurements, while force-spectroscopy averages single measurements of individual molecules.

Nevertheless, force spectroscopy directly and uniquely allows access to the most probable adhesion force, F, the potential width, Δx, and the unbinding energy, ΔG_{off}. This is complementary information to the equilibrium constant, K_D, and the off-rate, k_{off} (Morfill et al., 2007). For each reliable force experiment, the temperature and all of the viscoelastic constraints of each experimental setup have to be taken into account. The experimental setup includes the hard substrate over the molecular anchor (spacer included), the complex itself, the second anchor (spacer), and the cantilever with a known spring constant (see Figure 9.1). In a common first order approximation, an effective spring constant is calculated by the instruments' spring constant multiplied by the pulling velocity. The common approximation of the loading rate as the spring constant multiplied by the sensor velocity only holds for a rigid and stiff connection of the binding partners to the substrate and the force sensor. Any molecular spacer in series to the bond with elastic properties in the range of the force sensor or softer will change the loading rate in a sometimes nonlinear manner (Rief et al., 1997b). This is numerically adjustable if a model can represent the mechanical behavior of the spacer. With such a model of the setup's viscoelastic properties, the characteristics of the bond (potential width, Δx, and depth, ΔG) can be evaluated precisely (e.g., WLC-model as shown later).

9.3 Mechanical Properties of Single Molecules

According to the second law of thermodynamics, polymers like DNA or proteins maximize their entropy by relaxing into the energetically lowest conformation (random coil or even specifically folded proteins). Applying an external force to the ends of such a polymer increases the end-to-end distance, x, to an energetically less favored conformation with decreased entropy. This less-favored conformation generates a restoring force F due to the reduced entropy.

9.3.1 Entropic Polymer Elasticity (the Worm-Like Chain Model)

A simple model for such a molecule is the freely jointed chain (FJC) model, consisting of N segments of the length d* (Figure 9.6).

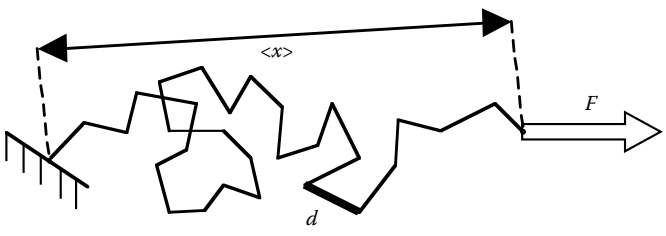

FIGURE 9.6 Sketch of the FJC model: Force F, end-to-end distance <x> and length of each chain segment d.

* A DNA single strand consists of phosphate groups with a connecting sugar ring (d = 5.7 Å), containing a base.

From thermodynamics, we can derive the average end-to-end distance $<x>$ under an external Force F as a partial derivative of G with respect to F at a constant temperature T:

$$<x> = -\left(\frac{\partial G}{\partial F}\right)_T = -k_B T \frac{\partial \ln(\boldsymbol{Z}(F))}{\partial F}$$
$$= Nd\left(\coth\left(\frac{Fd}{k_B T}\right) - \frac{k_B T}{Fd}\right) = Nd\boldsymbol{L}\left(\frac{Fd}{k_B T}\right) \qquad (9.7)$$

G is the free energy of the polymer conformation
$\boldsymbol{Z}$ is the partition function
$\boldsymbol{L}$ is the Langevin function

In order to apply this function to a measured force curve of a stretched polymer the inverse Langevin function describes the average force $<F>$ that is required to extend the end-to-end distance x:

$$<F(x)> = \frac{k_B T}{d}\boldsymbol{L}^{-1}\left(\frac{x}{Nd}\right) \qquad (9.8)$$

Assuming a semi flexible chain with a bending stiffness B, the characteristic length p can be defined as persistence length: $p = B/k_B T$. For forces $F \gg k_B T/p$, an approximation known as worm-like chain (WLC) model holds:

$$F(x) = \frac{k_B T}{4p}\left(4\frac{x}{L} + \frac{1}{(1-(x/L))^2} - 1\right) \qquad (9.9)$$

$L = Nd$ is the overall length of the polymer backbone. Other approximations for polymers with different properties are the freely rotating chain (FRC) and the freely jointed springs (FJS) model (Hugel et al., 2005). The result of fitting a polymer model to a force distance trace gives the typical persistence length* and the overall length of the polymer's backbone, respectively (Rief et al., 1997a; Oesterhelt et al., 2000).

9.3.2 Single Molecule Experiments

Many force measurements of the elastic properties of single molecules have been performed (Butt et al., 2005). As mentioned before, the design (temperature, loading rate, spring constant etc.) of such an experiment is important to gain useful results. In the following section, we will focus on the reaction pathway of the separating receptor–ligand complex and the influence of the position of the "molecular handles" on the measured force.

An external force might define an "artificial" reaction pathway to a complex (arrow in Figure 9.7) over an activation barrier invisible for calorimetric measurements following along the "natural" pathway. This barrier might appear only in force measurements at increasing loading rates. At slow loading rates close to the natural off-rate (light gray trajectory), this barrier might stay undetected, whereas at higher loading rates it is measured (darker trajectories).† A reaction coordinate perpendicular to the sketched one Figure 9.7 would not explore this barrier even at high loading rates.

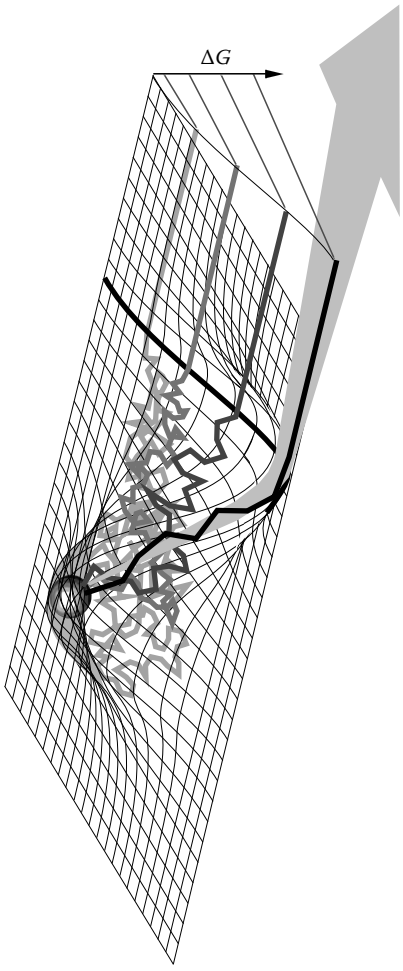

FIGURE 9.7 Sketch of a complex bound in a potential valley with an activation barrier (ΔG). Unbinding trajectories with increasing loading rates light to black become increasingly restricted to the reaction coordinate (big arrow) over the barrier by the external force.

9.3.2.1 Hands-on Molecules (DNA)

Measurements of the adhesion force between two individual DNA strands show us that the relation between the binding energy, ΔG, and measured force, $F(f)$, is not trivial, but nevertheless easy to understand.

In Figure 9.8, force spectroscopic experiments stretching a double stranded DNA molecule are shown at different velocities.

Whereas the force curves are similar until the end of the force plateau at all velocities, a hump appears at increased velocities at the

* Does not necessarily correlate to the physical length of the polymer segment.

† An additional reason for the higher forces in the MD simulations at high loading rates is the appearance of such barriers that otherwise are circumvented at normal velocities.

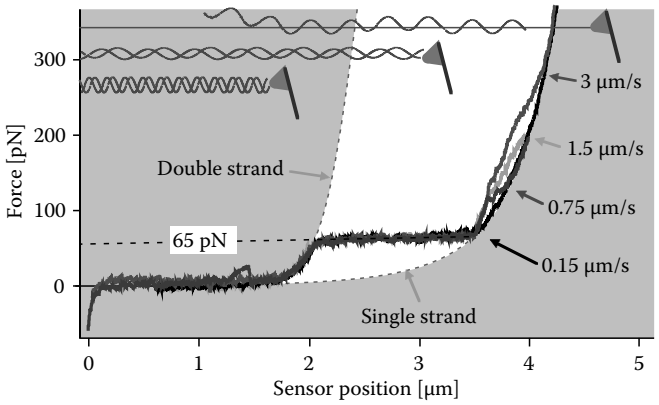

FIGURE 9.8 Four force experiments stretching a 2 µm long DNA double strand at different velocities (3, 1.5, 0.75, and 0.15 µm/s). A sketch of the DNA molecule fixed between the substrate and the force-sensing cantilever tip depicts the three stretching regimes. First regime: the double stranded DNA is stretched (along the dotted gray borderline) up to the second regime. The second regime (white background) links to the third regime via a force plateau at 65 pN (dotted black line). The third regime stretches a single DNA strand (along the dotted gray borderline). The dotted gray borderlines are WLC-fits to the force curve.

end of the plateau. Corresponding to Figure 9.7, an activation barrier becomes visible here that might be related to the friction that occurs while separating and unwinding the two strands at high velocities.

In the first regime, the two strands are wound up well and are stably connected to a double strand by the Watson–Crick base pairs until the force increases up to 65 pN. Now, the DNA undergoes structural changes and the strands start to separate until the end of the force plateau. This resembles a phase transition like a melting process to single stranded DNA. This pronounced plateau is a transition in thermodynamic equilibrium; thus the force does not depend on velocity.

If we consider the same experiment (as in Figure 9.8) with the force sensor attached to the blue strand, while the red strand stays attached to the substrate (shear mode), the experiment would terminate at the end of the 65 pN plateau: As soon as the two strands are separated, the connection to the substrate is lost, the force drops to zero and no single strand is stretched further.

Here, we understand that the mount for the handles connecting the molecules to the force spectroscopy experiment determines the reaction pathway. DNA is an ideal molecule for explaining the effect of the molecular handles in force spectroscopy, as three kinds of elucidating force experiments are possible:

The single strand stretch mode, where the handles are only connected to one strand at opposite ends (Figure 9.8).

The shear mode, where the handles are connected to either strand at opposite ends (Figure 9.9 left).

The zipper mode, where the handles are connected to either strand at the same end, as presented in the next example (see Figure 9.9 right).

In Figure 9.9, the DNA-oligomer sequence of the 30 base-pair DNA strands is identical in both modes. Thus, the binding energy, ΔG, is also identical, but the measured forces, even though pulled at the same velocity, are different. This example again shows: when opening a complex, the measured force is not correlated to the binding energy in a trivial relation. However, the forced unbinding experiments reveal new insights into the molecular structure of a bond. As expected, the length of the DNA-oligomer tunes the unbinding force (Figure 9.9 left). In the shear mode, a longer DNA-oligomer leads to an increased unbinding force but not higher than the 65 pN force plateau (BS-transition). In the shear geometry, the base pairs cooperatively resist the increasing force by equally distributing the overall force among each other. The shear potential is deep but the length is just a few Ångström. In the zipper mode, the full force is loaded sequentially to a single base

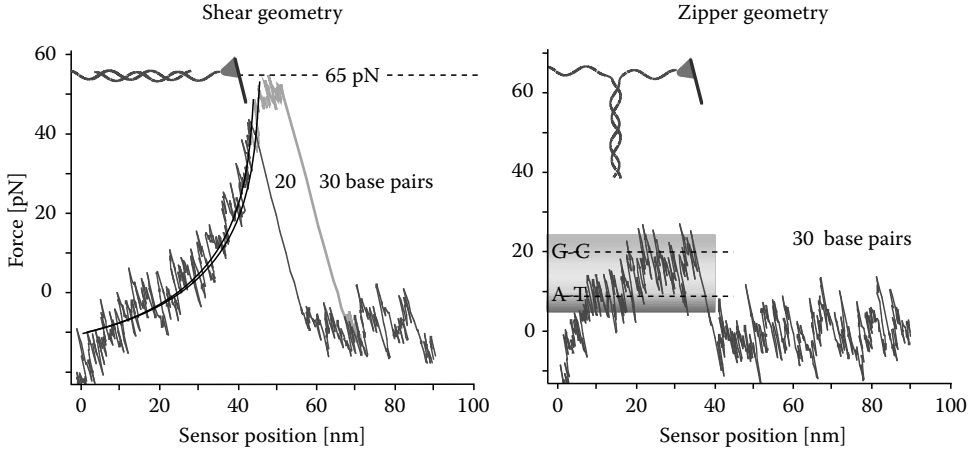

FIGURE 9.9 Unbinding force curves of DNA oligomers in the shear mode (dark curve 20 and gray curve 30 base pairs) and in the zipper mode (right curve 30, base pairs). Black lines represent WLC fits to the force curves. In the zipper mode, the force balances between 9 pN (A-T base pairing force) and 20 pN (G-C base pairing force). (From Rief, M. et al. *Nat. Struct. Biol.*, 6, 346, 1999; Courtesy of Zimmermann, J. and Kufer, S.)

pair, one by one. The resulting forces are dominated by the base pairing forces of AT = 9 pN and GC = 20 pN.* The zipper potential is shallower, but its length directly corresponds to the length of the DNA. Looking at this example, we easily understand why the result of a force spectroscopy experiment strongly depends on its design (where are the handles fixed?). In terms of force spectroscopy as an alternative technique to determine ΔG this is bad news, but it can be useful to understand nano structures, molecular geometry, and mechanics (Dietz and Rief, 2006; Puchner et al., 2008a). DNA provides three force standards: in the shear mode, a long DNA will clamp the maximum force at 65 pN, in the zipper mode a DNA that is purely composed from AT base pairs clamps the force at 9 pN, and if it is purely composed from GC base pairs at 20 pN. A sequence of hierarchically designed DNA force experiments incorporating one single DNA 20-mer single strand on the cantilever tip that matches in shear geometry to a transporter strand immobilized with a remaining sequence in shear geometry to a substrate yields a molecular cut and paste apparatus† (Kufer et al., 2008).

9.3.2.2 Receptor–Ligand Interaction Forces of the Biotin–Avidin Complex

Receptor–ligand interactions and intermolecular recognition are essential for life. Typically, biomolecules interact in a non-covalent manner. They are meant to separate again so that they can be reused again.‡

The first non-covalent interaction that was studied with force spectroscopy, the avidin–biotin interaction, is also one of the strongest. Biotin, a small peptide (Vitamin H) meanwhile became commonly used as a strong non-covalent standard linker (together with the tetrameric protein avidin or streptavidin) for biomolecular investigations (labeling, functionalization, or immobilization).

In less than 10 years of its invention, the AFM (Binnig et al., 1986) turned out to be a tool to obtain high-resolution images of atoms, molecules, and living cells (Radmacher et al., 1992), and pioneering work on intermolecular force measurements was done. The biotin–avidin bond was the first to be studied by AFM force-spectroscopy (Florin et al., 1994). Consequently, the separation of these interacting molecules was the first to be calculated by MD simulations initialized by Grubmüller et al. (1996). At that time, molecular dynamic simulations of a few picoseconds were extremely time consuming and the experimental timescales of milliseconds were still hard to address.

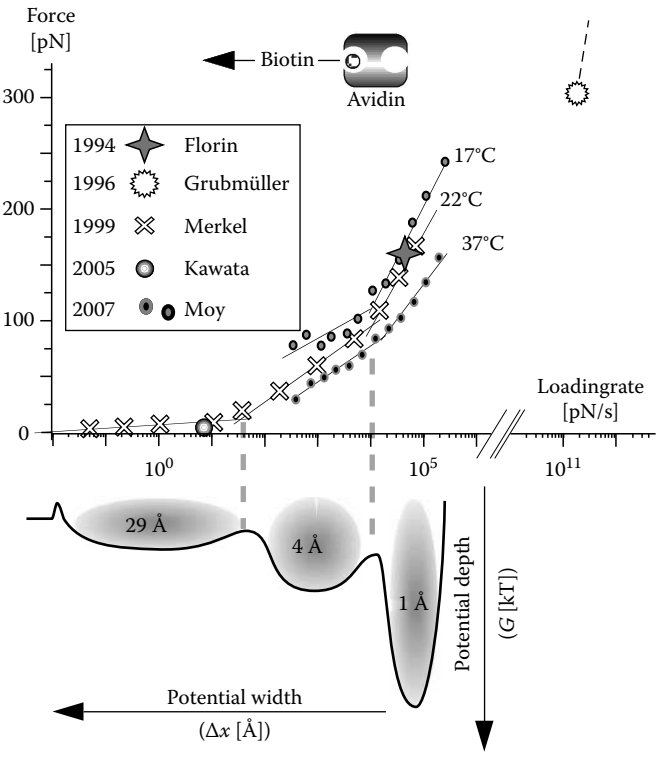

FIGURE 9.10 Investigations on the biotin–avidin interaction force plotted against the logarithm of the force-loading rate pioneered by AFM force-spectroscopy (Florin) and by early molecular dynamic simulation (Grubmüller, dotted line connects to further points out of the graphics range). Thorough studies confined the theory of this molecular bond by bio-force sensors (Merkel), by optical trap (Kawata), and by AFM (Moy, who also revealed a temperature dependency). Line fits indicate distinct regimes of the intermolecular bond: A schematic drawing of a possible potential landscape representing these regimes of the biotin–avidin interaction derived from Schulten et al. is sketched below the graph and outlined in Figure 9.11.

The most coherent picture of the biotin–avidin interaction is presented by Merkel et al. (1999), Rico and Moy (2007), and Isralewitz et al. (2001). The resulting potential landscape of the biotin–avidin interaction is schematically indicated in Figure 9.10. The very shallow and long ranged part (29 Å) of the potential is only accessible at slow loading rates (below 40 pN/s) and with very soft spring constants (<1 pN/nm) of BFS or OT.§ (A list of the spring constants from the experiments in Figure 9.10 is given in pN/nm [instrument]: Florin 39 [AFM], Grubmüller 2800 [MDS],¶ Merkel 0.1–3 [BFS], Moy 10 [AFM], and Kawata 0.045 [OT].)

* Unfortunately, the thermal energy of the Brownian motion exceeds the signal of the individual separating base pairs and defeats reading the DNA sequence with this technique.

† The free single-stranded end of the 50-mer transporter DNA sticking to a substrate in the 20-mer zipper geometry is picked up by the stronger force of the 20-mer shear geometry on the cantilever tip. The transporter DNA finally is transferred to a matching single strand 30-mer on another substrate in a force experiment between the stronger 30-mer shear geometry on the substrate and the 20-mer shear geometry on the cantilever.

‡ This does not hold for the so-called suicide-couplers; they covalently bind. Once bound, they will never open again (Kufer et al. 2005).

§ The lower force of the OT measurement might be due to a local heating above room temperature by the laser trap.

¶ The molecular dynamic simulations are performed at very high velocities in a completely different time frame (picoseconds instead of milliseconds). The mechanical properties of the molecular bond are different and the forces quite high and even up to nN, as indicated by the dashed line in such high velocities are inaccessible for the force measurements so far due to the hydrodynamic effects.

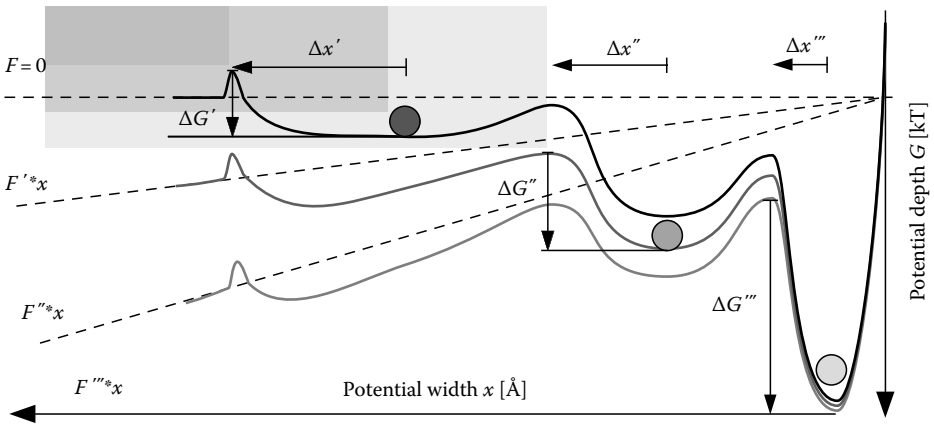

FIGURE 9.11 The three valleys of the biotin–avidin potential landscape in thermodynamic equilibrium without external force are sketched in black. Applying an external force tilts the energy landscape by a factor F^*x as sketched in grey. The shallow $\Delta x' = 29$ Å wide, part of the potential with an energy barrier height of $\Delta G_{off}'$ is probed in the force window $0 \le F \le F'$. An inner energy barrier $\Delta G_{off}''$ becomes "visible" behind the lowered barrier $\Delta G_{off}'$ in the force window $F' \le F \le F''$ that tilts the potential further. Now, the part of the potential with the width of $\Delta x'' = 4$ Å is probed behind that barrier. Further tilting the potential landscape, the energy barrier $\Delta G_{off}'''$ finally surmounts $\Delta G_{off}''$ and the last part of the potential landscape $\Delta x''' = 1$ Å is probed at forces $F \ge F''$.

The intermediate potential valley (4 Å) is represented by the steeper slope in the plot and the deepest and narrowest part of the potential (1 Å) is represented by the steepest slope to the right-end at loading rates above 10 nN/s.

Literally, this loading rate dependent behavior of the force regimes can be visualized (see Figure 9.11) by a potential tilt (F^*x) through the applied force. This picture is directly derived from the Van't Hoff–Arrhenius equation (Equation 9.6) under external force.

From a physicist's point of view, it is favorable to use spacer molecules that are well represented by models (WLC, FJC, etc.) for studying molecular interactions by force spectroscopy. Here it is possible to exactly recalculate the contributions of the incorporated molecules from the data. However, does this represent the "natural" situation of the investigated complex? The next example shows a complex of interest that is immobilized, as naturally produced, on a bacterium. Unfortunately, this natural spacer (the P-pilus) has a complex force-extension characteristic and cannot be described by a basic thermodynamic model!

9.3.2.3 The PAP-G–Galabiose Bond: Single Molecule Force Spectroscopy on a Cell

In this example of the force measurement between the galabiose and the PAP-G molecule, we study a system that was designed naturally for an external loading force. The P-pilus is a structure of PAP-units that are non-covalently linked to each other like a row of matching pieces of a puzzle. The PAP-units additionally are stacked together, forming a stiff helical rod. At the very tip of the P-pilus, the adhesion molecule PAP-G specifically binds to the galabiose on the surface of an epithelial cell of the urinary tract. The question of how to correctly apply the handles to the receptor ligand complex is solved by itself, because we perform the experiment as close to the real situation as possible. The galabiose is covalently linked to the PEG spacer on the AFM cantilever at the same side-group where it is *in vivo* linked to the glycocalix of a cell membrane. The PAP-G unit remains linked to the *Escherichia coli* bacterium as it is assembled on a P-pilus. A typical force-extension plot of a P-pilus is shown in Figure 9.12 with a highly reproducible pattern for all velocities: a plateau at 27 pN, followed by a steeper shoulder and then a WLC-like behavior. With a numerical reproduction of this curve, the load to the bond during an experiment can be simulated in a Monte-Carlo calculation. Together with the Bell–Evans model, a certain set of parameters for the potential width $\Delta x = 7 \pm 1.5$ Å and an off-rate = 8^*10^{-4}/s resembles the measured force distribution correctly (Figure 9.12). As we would expect from the previous consideration, the unbinding probability at 27 pN is increased because the bond is probed a few seconds in the long unstacking plateau at 27 pN. The most probable rupture force at 48 pN matches the force range of the transition 2. In the force range above 100 pN, the PAP-units of P-pilus would start to disintegrate irreversibly (Lugmaier et al., 2008). With this mechanism, the *E. coli* bacterium tries to stick to a target cell. In case of shear flow, the *E. coli* might be flushed away because the connection to the galabiose would be loaded and each bond would open up one by one if the force would exceed 48 pN.* However, thanks to the P-pilus, the bond is loaded only at 27 pN for a while and all the neighboring bonds on the other pili are also loaded in parallel at 27 pN. It is the P-pilus' strategy to parallelize each of the PAP-G bonds, so that the overall force is not 48 pN in a sequence (like in the unzipping of DNA) but continuously N times 27 pN (where N is the number of the bound pili). If the end of the plateau is reached, the force increases slowly but steadily. The range of the

* *E. coli* might use a stronger bond with a stronger force, but then it would be hard to reopen the bond and to reuse it at another binding site or the pilus might irreversibly disintegrate.

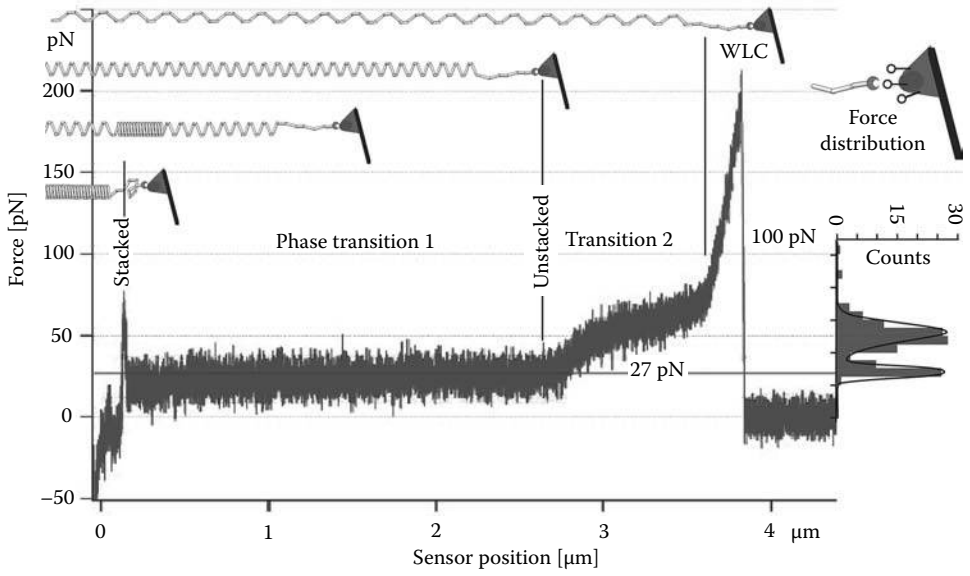

FIGURE 9.12 Force extension trace of a P-pilus and the force distribution between PAP-G and galabiose. A sketch of the unstacking pilus extended between the substrate (*E. coli*) and the galabiose decorated cantilever tip depicts four stretching regimes until the PAP-G unit releases the galabiose: first stretching the fully stacked pilus (left of the "stacked" line). Second coexistence of stacked and unstacked (phase transition 1) until the third phase: fully unstacked pilus undergoes a second transition (transition 2). The fourth phase behaves like a worm-like chain (WLC). The force distribution (histogram to the right of the unbinding forces) shows two peaks at 27 and 48 pN fitted by a Monte-Carlo simulation (black line).

transition 2 might be enough to add up the further increased force from some other P-pili reaching the transition 2. Since the P-pilus is a very "expensive" structure for the *E. coli* bacterium, the galabiose bond is released before forces above 100 pN could damage the integrity of the pilus. The PAP-G-hook is pulled back and sticks out on the stiff stacked pilus, waiting to bind to a next galabiose molecule.

Analogous to the *E. coli* experiment, the next chapter presents approaches for conducting force measurements between interacting molecules in their natural environment—the membrane of a living cell.

9.4 Force Spectroscopy on Living Cells

With some effort, the receptor and adhesion molecules of cells can be isolated and purified for single molecule force experiments. Some molecules cannot become covalently linked to the force sensor. Membrane-anchored molecules, in particular, often turn out to be insoluble in water. Immobilizing such (trans-) membrane proteins in artificial lipid membranes (supported bilayers) on a substrate is an alternative to gain access to membrane proteins with force spectroscopy (Dewa et al., 2006).

As an alternative, in this section, force measurements between single molecules and the living cells as well as force measurements between living cells at single molecular resolution will be described. The interacting molecules are provided in the "correct conformation" by the cell and the force is coupled into the molecules by the "natural handles." This opens up a broad field of study of cellular mechanisms and strategies that tune the adhesion strength of a cell at the molecular level (Parot et al., 2007; Helenius et al., 2008; Ludwig et al., 2008; Schmitz and Gottschalk, 2008; Selhuber-Unkel et al., 2008). The cell adhesion molecules of the integrin family are prominent examples for cellular adhesion regulators (see page 9-14). As the cell, reacting to its environment, might change its adhesion, a cell adhesion experiment can even serve as a reporter for the function of pharmaceutics (drugs, hormones, and chemokines) that trigger an intracellular reaction with an impact on adhesion (Schmitz and Gottschalk, 2008). Most mammalian cells are optimized to metabolize at 37°C. To conduct an AFM experiment at temperatures unequal to the ambient room temperature attracts drift effects to the temperature sensitive force sensor. Unfortunately, the advantages of studying the molecular interactions between single molecules located in cellular membranes are counterbalanced by the fact that there will never be a perfect model of the very complex cell that serves as a "spacer" between the substrate and the molecule or the molecule and the cantilever, respectively. Each cell might react differently due to the cell cycle, the last feeding period, the temperature changes during preparation, and the exerted force. The cell as "spacer" contains several billions of molecules. The complex interplay of all of them renders the mechanical characteristics of the cell, that is, the linker between the adhesion molecules and the substrate, and the force sensor, respectively.

From solid-state physics, we can borrow classic models about viscoelastic bodies and approximate them to the mechanical answer of a cell in a force experiment.

9.4.1 Cell Mechanics (Theory)

In a simplified way, the major players in cell elasticity are the cytoskeleton (with its actin filaments, microtubules, and intermediate filaments), the cytosol, and the cellular membrane. The cellular membrane separates the intracellular from the extracellular space and incorporates the adhesion molecules. Some cells have smooth surfaces, others expose "fingers" (filopodia or microvilli) protruding the membrane by actin filaments (Alberts et al., 2002). In a typical force experiment, the relaxed membrane easily adapts to the shape of the indenting cantilever. The membrane supporting cytoskeleton starts to exert a pronounced elastic counter force to the further indenting cantilever tip compared to the weak contribution of the compliant lipid membrane.

On a millisecond timescale, the elastic property of the cell is predominant, but already in the second timescale, viscous and plastic deformations of the cellular components occur. To describe the cellular reaction to the indenting cantilever, general concepts of modeling viscoelastic properties of matter from solid-state physics are used. Here, we focus on a elasticity model by Heinrich Hertz that was developed originally for two interacting elastic spheres [Hertz model (Hertz et al., 1882)] and on some basic arrangements of dashpots and springs (Kelvin-, Maxwell-, and Voigt-model) representing viscoelasticity models (Fung, 1993).

In a very simplified way, one can interpret the force interaction between two cells as the interaction of two elastic spheres (see Figure 9.13). By a few approximations, the general Hertz-model can be reduced to the following equations:

Equation 9.10 describes a compliant spherical object (radius: R, elastic modulus E and the Poisson ratio: ν) indented at a distance z by a rigid plane (= a rigid sphere with an infinite radius):

$$F_{\text{sphere}} = \frac{4}{3}\sqrt{R}\cdot\frac{\mathbf{E}}{1-\nu^2}\cdot\sqrt{z^3} \tag{9.10}$$

For symmetric reasons, the same Equation 9.10 is valid for a rigid spherical object (radius: R) indenting an elastic object with a plane surface by a distance z. A second equation describes a rigid conical object (semi-angle of the cone: α) indenting a plane compliant object by the distance z (this holds for a typical cantilever with a conical tip indenting a cell, that at the tips' scale for small indentations approximately has a plane shaped surface):

$$F_{\text{cone}} = \frac{2}{\pi}\tan(\alpha)\cdot\frac{\mathbf{E}}{1-\nu^2}\cdot z^2 \tag{9.11}$$

In most of the cases, the Poisson ratio ν can be set to 0.5 that represents a homogenous and incompressible elastic medium.

The Force F is proportional to the 3/2 power of the indentation z in Equation 9.10 and to the square of the indentation z in Equation 9.11.

From this static Hertz model we can derive the Young's modulus E of a cell from each force curve when approaching the cell with the force sensor (Radmacher, 2002; Wojcikiewicz et al., 2004; Lamontagne et al., 2008).

The viscoelasticity of a cell can be evaluated better by adding viscous elements to the description. An ideal viscous element creates a force that is proportional to the applied velocity with inverse orientation. In a typical experiment, the viscous drag force is constant because the force sensor travels with a constant velocity (changing sign from approach to retract after the contact with the cell).

Figure 9.14 depicts force-versus-distance plots of virtual AFM force experiments at constant velocity on idealized models composed from dashpots and springs. An ideal Hooke's spring would travel from zero with a constantly increasing force, whereas an ideal dashpot would jump with the velocity to a force according to the viscosity at this velocity and stay constant at

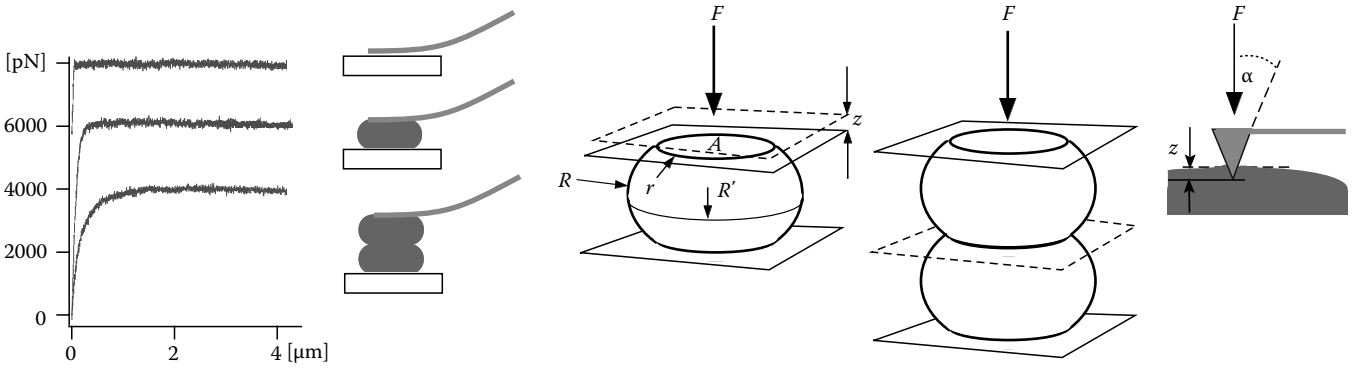

FIGURE 9.13 The elastic modulus E can be derived from the analysis of the indentation force curves, using the Hertz model. The indentation force curves are derived from a plain cantilever indenting a rigid plane substrate (1), a tipless cantilever indenting a red blood cell (2) and a red blood cell immobilized on a tipless cantilever indenting another red blood cell (3). In the middle, the geometrical schematics that are used in the Hertz-model are shown: the indenting force F, the indentation depth z and the radius of the sphere R. (contact surface A, contact radius r and extended radius R' are not needed in the simplified Hertz-model shown here). To the right the geometry for the conical indenter is sketched. (Modified from Benoit, M. and Gaub, H.E., *Cells Tissues Organs*, 172, 174, 2002.)

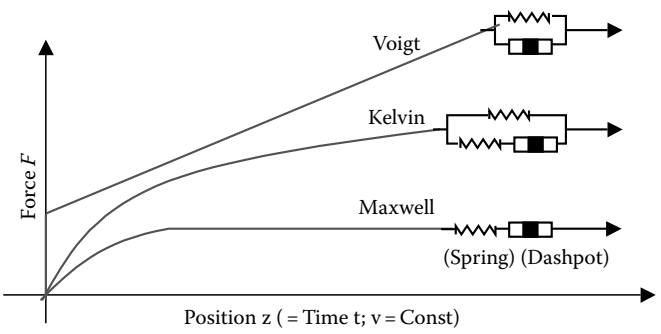

FIGURE 9.14 Force distance traces of the elastic bodies (as depicted from above: Voigt-model, Kelvin-model, and Maxwell-model) reacting to an elongation constantly increasing with time.

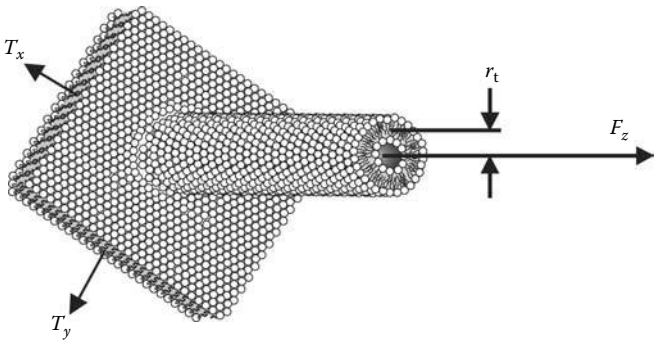

FIGURE 9.15 A schematic drawing of a membrane tether with the radius, r_t, pulled from lipid bilayer. The membrane tension is represented by T_x and T_y and the force F_z pulling the membrane tether and its length l_t is measured by the AFM.

this force. The Voigt, Kelvin,* and Maxwell model are combinations of springs and dashpots and are a first choice for describing the viscoelastic properties of cells.

In some typical cell-adhesion force curves shown in Figures 9.20, 9.21, and 9.26, elucidating the huge variety of viscoelastic responses of the cellular "spacer" signatures of the presented models might already be identified. To get a clearer picture of the mechanics behind these traces we need to give more attention to the cellular spacer.

9.4.1.1 Tether

A typical pattern in which cells perform in combination with adhesion, are lipid membrane tubes called "tethers" (Waugh and Hochmuth, 1987). Tethers are pulled out from the membrane around a membrane-anchored adhesion spot when the cantilever is retracted while the adhesion spot is still intact (Figure 9.15).

A membrane tether forms as a lipid bilayer tube with typical diameters of 10–200 nm, counterbalancing the energies of the membrane's tension and the membrane's curvature (Raucher and Sheetz, 1999; Marcus and Hochmuth, 2002; Sun et al., 2005; Harmandaris and Deserno, 2006). The diameter also depends on the lipid and protein composition of the membrane, on the ambient temperature, and on the amount of molecules (e.g., actin filaments) that are pulled within the tube. Neuronal cells tend to pull long tethers of up to millimeters until they detach![†] (Hochmuth et al., 1996).

A typical membrane tension T_{cell} for cells is usually about 15 fN/nm (Discher et al., 1998) that induces an equilibrium tether force F_t in a tether of the radius r_t (r_t is defined in the center between the two lipid bilayers)

$$F_t = 2\pi \cdot r_t \cdot T_{cell} \tag{9.12}$$

The stiffness of the lipid membrane does not favor a narrow curvature and as a consequence of the interplay between the membrane stiffness, B ($1.8*10^{-19}$J)[‡] (Hwang and Waugh, 1997), the membrane tension, T_{cell}, and the axial tether force, F_t, a formula for the typical tether radius, r_t, was found (Waugh and Hochmuth, 1987):

$$r_t = 2\pi \frac{B}{F_t} \tag{9.13}$$

By combining Equations 9.12 and 9.13 the tether force of a lipid membrane tether, depending on the membrane tension T_{cell} is calculated:

$$F_t = 2\pi\sqrt{B \cdot T_{cell}} \tag{9.14}$$

The typical physiological membrane tension (T_{cell} = 15 fN/nm) would result in a typical steady-state axial tether force F_t of 9 pN at a radius, r_t of 110 nm. When a tether is pulled at constant velocity, a steady flow of lipids into the growing tether is recruited from the cell membrane. An additional (constant) force adds up proportional to the pulling velocity and is composed of the friction and the viscosity at the tether's foot. Consequently, the axial tether force, F_t, at the tip is higher than the one calculated from the tension in the cell membrane. At membrane (hyper) tensions of T_{cell}^{max} between 2 and 20 pN/nm, a lipid membrane would disintegrate (Evans et al., 2003). Equation 9.14 calculates the maximum force, F_t^{max} that a cellular membrane tether could withstand between 120 and 300 pN. Even though the bilayer might withstand tether forces above 300 pN, the tether radius would come below 3 nm and the bilayer would collapse. The bending rigidity and the maximum membrane tension largely depend on the lipid composition and the ambient temperature (Sackmann, 1995; Seifert and Lipowsky, 1995; Heimburg, 2007).

* The Voigt and the Maxwell model can be represented by the Kelvin model if either the parallel spring is set equal to zero (Maxwell) or the spring in series to the dashpot is set indefinitely stiff (Voigt).

† This usually excludes neuronal cells from the force experiments, because no AFM piezo will travel millimeters at a high resolution!

‡ The transition from fluid to solid phase of lipids in the membrane (induced by temperature, electrical potentials, and lipid mixtures) markedly can change the mechanical properties of the cellular membrane.

Tethers pulled from cells can vary in diameter and viscoelastic behavior. If actin bundles or membrane proteins are pulled within the tether or if the membrane tension, T_{cell}, is very low, the tether radius, r_t, can be increased to some hundred nanometers. If the tether radius exceeds 100 nm and several actin filaments are included, the distinction between the tether and the microvillus blurs.

9.4.1.2 Tether Model

Usually cells have a large reservoir of membrane to keep the membrane tension constant. Cells can refill lipids into the membrane from the caveolae and by exocytosis. (Sens and Turner, 2006). In a force experiment at constant velocity, we recognize a membrane tether by the almost constant force plateau in the force trace. A constant load is exerted to the bond(s) attaching the tether to the force sensor, while the small tube is pulled from the cellular membrane at constant velocity (see Figure 9.16). In an extreme case where the bond does not open until the membrane reservoir of the cell is used up completely, this constant force would increase (as indicated by the dashed line in Figure 9.16). Neurons in particular have a "never ending" membrane reservoir. In a first approximation, tethers behave like viscous elements due to the hampered viscous flow of the cell membrane through the foot of the tether. Tethers keep the force exerted to the bond constant according to the pulling velocity and thence the loading rate of the bond close to zero (= force clamp analogous to the BS-transition plateau of DNA in Figure 9.8). Compared to a steadily increasing force of an elongating spring, such a tether at constant force can maximize the adhesion energy of a bond that is strong enough to stand this constant tether force. Compared to a Hooke's spring, the energy (force times distance) increases quadratically with the pulled distance and the force linearly up to the level that breaks the bond. The tether keeps the force below that bond breaking level, while the energy increases only linearly but for a very long distance (like a releasing fishing line). As discussed above, *E. coli* and gram-negative bacteria lacking a lipid membrane as an outer layer had to develop the very complicated pilus structure to mimic the benefit of that viscous behavior of membrane tethers (Lugmaier et al., 2008).

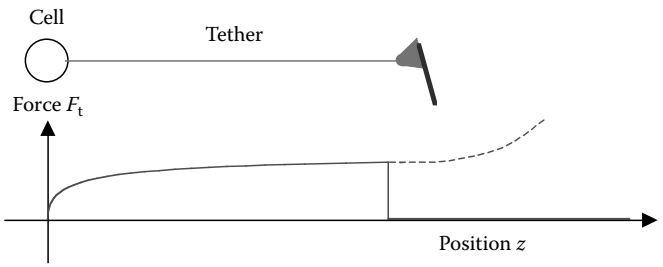

FIGURE 9.16 Tether schematics of a cantilever pulling a single tether from a cell and a typical force trace of a membrane tether. If a membrane tether is pulled from a small cell (platelet or red blood cell) with a limited membrane reservoir, the membrane tension would increase due to the limited surface area to cover the volume of the cell and the increased need for of membrane for the pulled tether. This would lead to an increased force as indicated by the dotted line.

Equipped with these simplified viscoelastic models, we will later see that from cell-adhesion force-spectroscopic experiments interesting results and conclusions can be drawn about molecular anchoring. First, we will look at the main players that all these efforts on modeling the cellular spacer were made for—the cell adhesion molecules.

9.4.2 Molecular Concepts in Cell Adhesion

Molecular biologists maintain a large and increasing library of known adhesion molecules and their molecular data and these entities are available for scientists all around the world via the Internet.

Unfortunately, some molecules, namely, the cell adhesion molecules, very often lose their natural behavior when they are extracted from the cellular membrane and transferred into experiments. In their natural environment, the cellular membranes are fixed either by a lipid anchor or by one or more hydrophobic transmembrane regions stabilized in the membrane. In a force experiment, basic lipid anchors can withstand forces of about 20 ± 10 pN (at a separation velocity of 5 µm/s). The strength of a lipid anchor depends on the lipid layer composition (Evans, 1998). Transmembrane anchors hold stronger forces (Oesterhelt et al., 2000) and additionally allow further attachment to the cytoskeleton inside the cell. Such transmembrane anchors can utilize conformational changes of the connected adhesion molecule in the extracellular space: induced by an adhesion at the extracellular region, a reaction at the intracellular region is triggered by a change in conformation (outside in signaling) (Pierres et al., 2007). The adhesive site of the molecule can also be tuned from inside the cell via the transmembrane anchor to the extracellular space (inside out signaling).

9.4.2.1 Adhesion Molecules

Adhesion molecules are divided into families and subclasses. In Figure 9.17 a few molecules and their reaction partners are depicted as examples.

Adhesion molecules can adhere to their partners in different ways classified as followed.

Homophilic: only molecules of the same kind can adhere to each other (csA and cadherins)

Heterophilic: the interacting partners are molecules of different kinds ($\alpha_4\beta_1$<->V-CAM-1)

Mediated: the interacting adhesion molecules need a third molecule to mediate adhesion ($\alpha_{2b}\beta_3$-fibrinogen-$\alpha_{2b}\beta_3$).

Some molecules can form multimers to enhance the adhesion or the selectivity with an analogous classification: homo multimerization (clustering) or hetero multimerization (integrins always occur as hetero dimers, the formation of lipid rafts is also seen as hetero multimerization)

Cell-to-cell and cell-to-surface adhesion involves a variety of different adhesion systems. Tight junctions form impermeable barriers within an epithelial cell layer. Adhesion belts (adherens junctions) and desmosomes (formed by cadherins and other proteins) serve to link to actin, intermediate filaments, and other

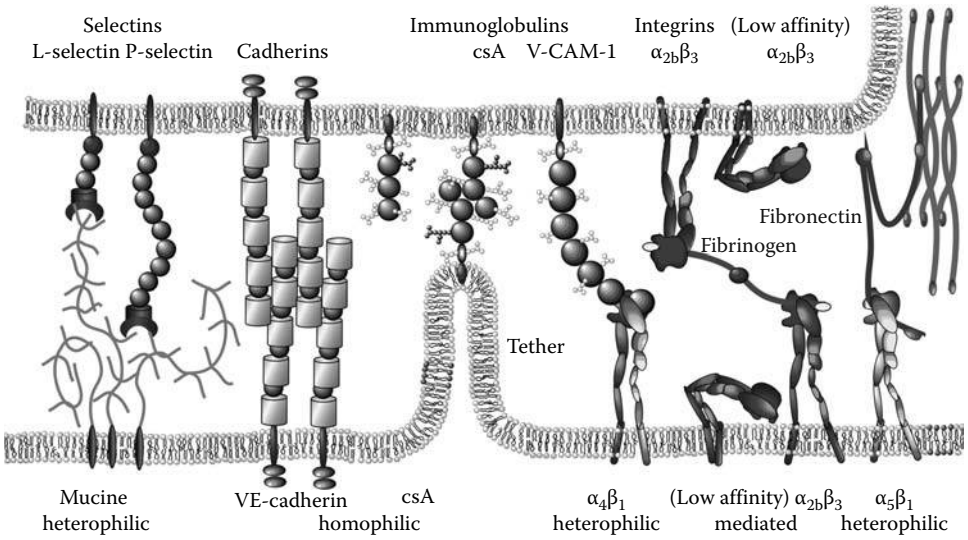

FIGURE 9.17 Survey of the most important mammalian cell adhesion molecules: Selectins, cadherins, members of the immunoglobulin superfamily (csA and V-Cam-1) and integrins. Cell adhesion molecules interact, homophilic, heterophilic, or use linker molecules (fibrinogen) to mediate adhesion between the adhesion molecules. The selectins specifically bind to glyco-proteins (mucins) cadherins form dimers and interact homophilically with another cadherin dimer. In a molecular cluster, they can multimerize to a very strong adhesion disk. Contact-site A (csA) and the vascular cell adhesion molecule (V-CAM-1) are representing the huge super family of the immunoglobulins. Integrins also form dimers like the cadherines, but heterodimers. They consist of an α- and a β-monomer and can change their affinity by changing their conformation (low affinity of $\alpha_{2b}\beta_3$). Fibronectin is a constituent of the extracellular matrix. The integrin recognizes the RGD peptide sequence of the fibronectin, of V-CAM-1, of fibrinogen and of all the other molecules specifically binding the integrins.

components of the cytoskeleton. Gap junctions formed by connexins allow ion exchange between cells. Selectins and integrins form specific connections to specific extracellular binding sites and mediate cellular recognition and targeted locomotion.

Integrins are interesting adhesive membrane receptors, as they are known to be individually tuned by the cell in adhesion strength (low, medium, and high affinity). They are therefore widely utilized by cells to mediate adhesion, cell sorting, and targeted migration. All integrins require divalent anions (e.g., Ca^{2+}, Mg^{2+}) for binding if they recognize a peptide sequence RGD (*Arg*inin-*Gly*cin-*Asp*aragin) in the binding partner. By shifting the concentrations of divalent anions in the medium, integrins artificially can be switched between affinity states: no divalent anions = low affinity, presence of Ca^{2+} = intermediate affinity, and presence of Mg^{2+} replacing Ca^{2+} = high affinity. Integrins are hetero dimeric transmembrane proteins: presently 19 α-monomers and 8 β-monomers are known in the human body. The RGD binding domain is located in the α-monomer. The combination of an α-monomer and a β-monomer so far results in 24 different known integrins specific to certain binding partners (e.g., $\alpha_5\beta_1$ specifically binds to fibronectin, $\alpha_6\beta_1$ to laminin, $\alpha_1\beta_2$ to I-CAM, $\alpha_4\beta_1$ to V-CAM…)

Most of the integrins at physiological salt concentrations are in an intermediate or low affinity state diffusing in the membrane. They either change to an adhesive conformation when diffusing into an activating part of the membrane where cytoskeleton-related molecules connect to the integrins' cytoplasmic part (inside out signaling). Integrins also change their conformation when sensing an external binding partner or an external force (outside in signaling). For example, the integrin's β_3 subunit binds via cytoplasmic talin to actin that is a constituent of the cytoskeleton. On the other hand, phosphorylation of the β_3 cytoplasmic tail by the cell prevents binding to talin. Additionally, the integrin changes into a conformation that releases a bound ligand from the extracellular integrin binding site (inside out signaling). The full functionality of integrins is definitely maintained only in an appropriate lipid membrane. Furthermore, the tuning of the integrins' affinity by the cell can be utilized as a reporter for adhesion-relevant processes inside the cell. Obviously, these molecules and their dependency on intracellular processes can only be investigated properly in a cellular membrane of a living cell.

9.4.2.2 Adhesion Strategies

Different strategies are possible for a cell to control its adhesion strength:

Avidity: How many binding competent molecules are available in the membrane to be accessed by the binding partner?

Affinity: How strong is the bond? Affinity is described, commonly, by the dissociation constant, K_D, or the off-rate. The unbinding force and the molecular bond potential (width Δx and depth ΔG) also represent the affinity in force experiments.

Anchoring: How is the adhesion molecule linked to the cell? Molecules freely diffusing in the membrane might reach the adhesion site faster than molecules restricted by a connection to the cytoskeleton. However, a pure lipid anchor holds approximately 20 pN only, whereas a transmembrane anchor with up to

approximately 100 pN is much stronger. The strongest group of anchors connects the intracellular domain of the adhesion molecule to the actin, tubulin or other filaments of the cytoskeleton with up to the nano-Newton range. The anchorage of an adhesion molecule defines the mechanical environment ("spacer") of the adhesion molecule. It controls the lateral motility in the membrane and the loading rate of the applied force to the adhesion site.

Clustering: This is a strategic combination of avidity, affinity, and anchoring that increases the affinity of an adhesion spot with a strong anchor to the cytoskeleton by multimerizing the binding competent adhesion molecules (desmosomes, gap junctions, tight junctions, and focal adhesion). Such a cluster can withstand forces of approximately 30 nN. Clusters contain a self-healing mechanism through the rebinding of broken bonds. Dissociating bonds are not pulled apart due to the neighboring molecules keeping the split partners in close proximity. Such a force can either rip a cell or the cluster apart. The molecular clustering resembles the unbinding experiment with the shear DNA: the adhesion strength of each single molecule adds up to one big de-adhesion event instead of opening (pealing off) one individual bond after the other (as in the zipper mode in Figure 9.9) (Besser and Safran, 2006; Erdmann and Schwarz, 2006). The cell has a wide variety of possibilities via the anchoring to influence the adhesion. An adhesion molecule anchored in an actin-rich protrusion (microvillus) exposed on its tip has a higher probability to probe any object coming close to the cell than the one on the retracted membrane parts would have. As already mentioned, a molecule purely sitting in the membrane is limited in its binding force to the strength of the membrane anchor, even though the affinity of the binding site might be much stronger. It will be either ripped out of the membrane upon the stronger adhesion or form a membrane tether. The cell can tune the level of the tethers' force plateau by the lipid composition and lipid rafts.*

9.4.3 Cell Adhesion (Force Measurements)

Cells are the smallest units of life. As individuals (amoeba), they adapted very well to the environment during evolution and now they have to adequately react to several actual environmental changes in order to survive. In multicellular organisms, cells started to become specialists for certain tasks (immune cells, neurons, endothelial cells, etc.) to better adapt to environmental changes or even change the environment altogether (to a better one?). Communication between the cells, sorting, migration, homing, and many other functions have to be maintained in the multicellular organism. Therefore, some cellular reactions are universal, while some are only present in heart muscle cells, inner ear cells, red blood cells, and so on. Thus, for cell adhesion experiments there is no universal protocol. In the worst case, a new protocol has to be elaborated for each cell type. Nevertheless, a few basic principles will be described in the following examples.

9.4.3.1 Force Sensor Preparations for Cell Adhesion Measurements

The problem of mounting the molecular handles correctly is solved by the cell, but now we have to face a general problem of cellular force spectroscopic experiments: how to immobilize cells?

Very recent and universal methods are based on the aspiration of the cell on a small hole in a substrate by a tiny pressure gradient (Pamir et al., 2008) or in a system of micro-fluidic channels (Ryu et al., 2008). Latest cantilever designs might even allow the aspiration of the cell to the cantilever in the near future (Godin et al., 2007). However, presently one has to immobilize a cell on the cantilever by an adhesive coating (Benoit, 2002). In Figure 9.18, the possible designs of cell adhesion force measurements are summarized.

In a classical AFM experiment, a bare cantilever is used for imaging a cell. This already allows the detection of the nonspecific adhesion to the material of the cantilever tip (e.g., Si (SiO), SiN, etc.). In general, soft cantilevers with a spring constant of less than 10 pN/nm and blunt (at least non-sharpened) tips, pyramidally shaped with radii larger than 20 nm, are recommended in connection with cells. Cells survive uncontrolled indentations of soft cantilevers more often than of hard cantilevers with sharpened tips. The AFM imaging resolution on soft and rough samples is reduced anyway, so a non-sharpened tip is not a regression. Presently the best cantilever marked for this purpose is the MLCT cantilever by Park Scientific (now distributed by Veeco Instruments). The spring constant is said to be 10 pN/nm, but due to fabrication uncertainties, this number might vary by more than 100%. Therefore, it is important to independently determine the spring constant of each cantilever. To probe more specific interactions, the cantilever can be functionalized with an adhesion molecule. At this point, one should be aware of the fact that plain coating of the cantilever in the solvated molecule leads to some major obstacles concerning force measurements:

- Denaturation of the molecule on the surface of the tip
- Bad orientation of the molecule on the surface of the tip
- Harvesting of the molecule from the surface of the tip by the cell during force measurements
- Nonspecific interaction of the cell with uncoated areas of the tip or denatured molecules on the tip

A proper functionalization of the cantilever covalently links the molecule of interest via a non-adhesive spacer (e.g., PEG) to the tip (page 9-10)

9.4.3.1.1 Single Cell on the Cantilever

For a "functionalization" of the cantilever with cells, the pure coating recipe is sufficient, since now the cell will be the surface with which the sample interacts. Depending on the cell type,

* Controlled temperature is a crucial prerequisite for reasonable cell adhesion measurements: The viscosity of the cellular membrane extensively depends on the temperature. Drastic changes in viscosity take place at the transition temperature from the liquid to the solid phase of the lipid bilayer (Heimburg, 2007).

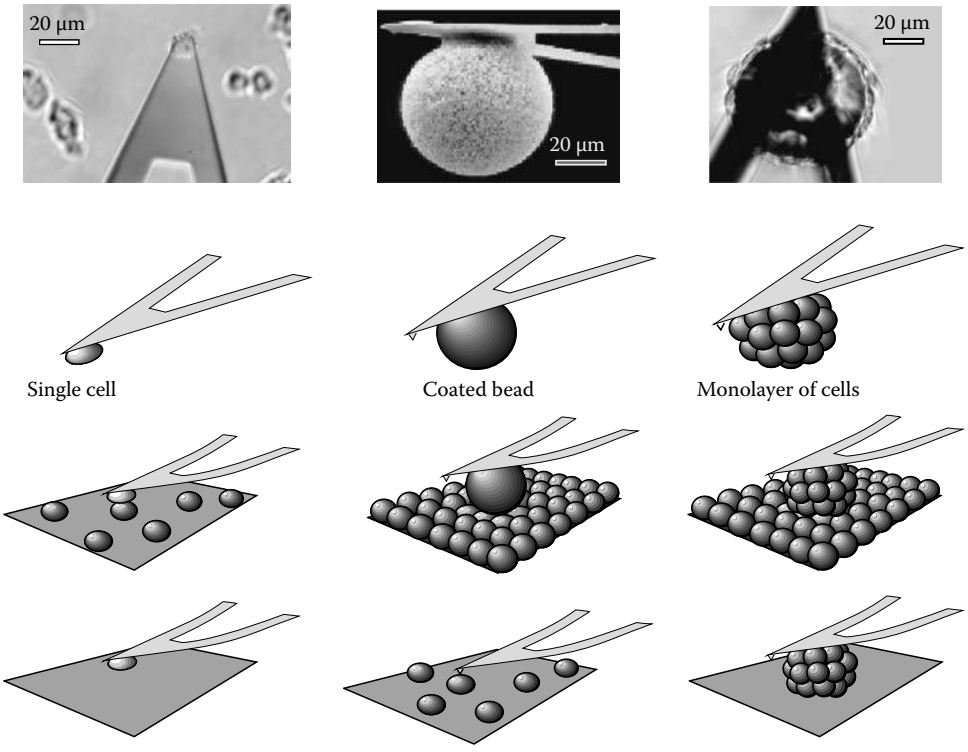

FIGURE 9.18 The left column of images: light microscopic image of a *D. discoideum* cell immobilized on a tipless cantilever. Other cells on the substrate are below the focus plane. Schematics below: cell functionalized cantilever, force measurements of single cells, and force measurement of a single cell to substrates. Middle column of images: REM micrograph of a sepharose bead glued to a cantilever. Schematics below: force sensor with microbead, force measurements between the bead and a cell layer. For the sake of completeness of the force measurement of a cantilever tip on single cells. Last column: light microscopy image of bone cells grown on a glass bead on a cantilever (focused at the center of the bead). Schematics below: cell layer functionalized bead, force measurements between two cell layers, and force measurement between cell layers with substrates.

polylisins, concavalin A, or fibronectin are among the good candidates for precoating the cantilever. With such a precoated (preferentially tipless) cantilever, a cell waiting on a weak adhering surface (e.g., BSA coated Petri dish) can easily be "fished" by a cantilever that is gently brought into contact with the cell for seconds. With tiny tweezers, the tip might be removed from the cantilever mechanically if no tipless cantilever is available.* The freshly attached cell might adhere more firmly to the cantilever after 1–10 min† before the "cell functionalized" force sensor is used for force experiments on a substrate (page 9-18), on another cell (Puech et al., 2006), and (page 9-21).

9.4.3.1.2 Sphere on the Cantilever

Adhesion measurements on confluent cell layers with a tipless cantilever often results in a badly defined contact area. One possible way of improvement is to glue a sphere (radius 5–50 µm) to the cantilever. Sepharose, Agarose, Latex, or glass beads can be glued to the cantilever by a drop (less than a pico liter) of two-component epoxy. Such a sphere functionalized with adhesion molecules can be useful to probe different cell layers in cell culture dishes. (page 9-20)

9.4.3.1.3 Cell Layer on the Cantilever

Finally, such a coated bead on the cantilever can be cultivated in a cell culture after gently injecting a couple of cells onto the bead on the cantilever.‡ After a few days, a cell layer grows on the sphere (see Figure 9.18 top right).

This configuration can be probed on surfaces or other cell layers (page 9-23).

The complexity of the cell adhesion experiments increases with the number of contributing cells and molecules. Starting with interactions between a single cell and a defined functionalized surface (e.g., cantilever tip or glass slide), followed by interactions between two individual cells, then between a cell layer and functionalized surfaces and finally multicellular interactions between cell layers.

* In this case, the spring constant of the triangular cantilever can be halved by pinching of the second leg in the same way as the tip.

† Do not lift the cantilever out of the liquid unless you want to remove the attached cell. Each detachment of the cell passivates the cantilever surface with remaining cellular membrane patches.

‡ As for all preparation steps the cantilever lays downside up in order to access the tip and to prevent damages to it.

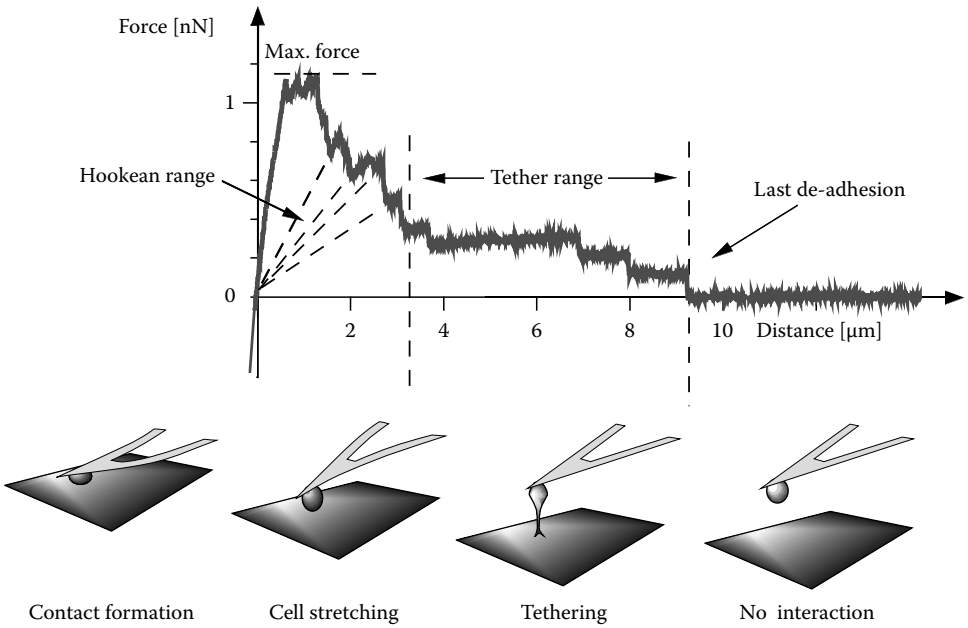

FIGURE 9.19 A typical force graph from a single-melanoma cell-adhesion experiment after a 1 min contact at 200 pN to a V-CAM-1 functionalized substrate at 37°C. The steep initial increase of the force reflects the predominantly elastic stretching of the whole cell. Around the maximum force, an increased number of intensive unbinding events take place. In the descending shoulder single de-adhesion steps become discernible with a force loading slope that is close to a Hookean behavior (indicated by dashed lines to the origin). Then in the tethering region, the slope is close to zero until the cell fully detaches from the substrate. The scheme below the force trace illustrates the situation of the cell in the force experiment. (Modified from Benoit, M. and Gaub, H.E., *Cells Tissues Organs*, 172, 174, 2002.)

9.4.3.2 Single Cell-to-Surface Measurements

The adhesion force measurement of a single cell to a substrate is the most prevalent experiment, as it involves the complexity of only one cell. Either a functionalized surface of the cantilever tip on a cell or a cell-functionalized cantilever on a functionalized substrate realizes this configuration. For example, a cantilever functionalized with the lectin (*Helix Pomatia*) that specifically recognizes red blood cells of the blood group A, repeatedly measured adhesion forces, while scanning a sample of mixed red blood cells of group A and O (Grandbois et al., 2000). With this label-free technique, individual red blood cells of group A were localized on this sample. In the MAC-mode such images of cells are obtained very fast at high resolution (Schindler et al., 2000).

To test the adhesion behavior of the same cell on different substrates, the second configuration with a single cell on the cantilever (Figure 9.19) is particularly useful. From the complex force traces of a cell-adhesion experiment, scientists usually extract the following numbers (Franz et al., 2007):

The *initial slope* is the approximately linear first increase of the adhesive force (Figure 9.19). It represents the elastic elements of the cell (Figure 9.20).

The *maximum adhesion force* indicates the highest force in the force plot. This is a rough first approach to quantify the adhesion strength.

The *slope prior to a de-adhesion event* is a hint for the actual cellular "spacer." A slope close to zero indicates a tether, whereas a steep slope results from a strong spacer. If the extrapolation of the slope comes close to the origin* of the force distance plot, the spacer behaves like a Hookean spring.

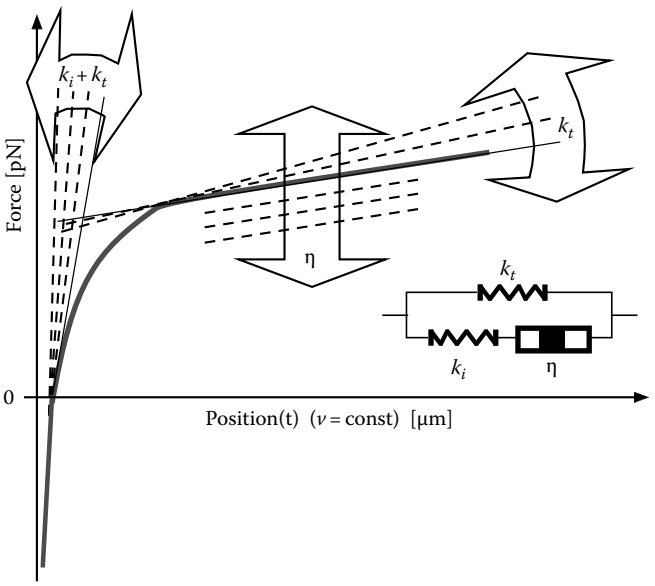

FIGURE 9.20 How elements of the Kelvin-model tune a force graph of a tether at constant pulling velocity.

* Defined as the intersection between the force-zero line with the first increase of the force plot.

The *distance from the original cell surface* (origin) of a de-adhesion event allows an upper estimate for the force loaded to the bond opened at this de-adhesion event.

The *force step size* of a de-adhesion event allows for a lower estimate of the actual unbinding force. Solely the very last de-adhesion event is an exact measure of the unbinding force, the de-adhesion events before might have been higher but appear lower due to the still existing force connections mediated by possibly non-independent cellular components between the surface and the cantilever.

The *area* spanned by the force trace above the zero line has the dimension of energy. It rather reflects the energy dissipated by the separation of the cell from the surface, than an "adhesion energy" of the molecular bonds of the tested surface.

The *adhesion rate* is not determined by a single force measurement. It is the fraction of force curves with adhesion events from a whole set of at least 50 force curves (e.g., all force measurements with contact times of 2 s on a substrate without adhesion molecules).

The *bond formation rate* is determined by the number of recognized adhesion events per force curve. From the measurement in Figure 9.19 this number is not determined. It might be registered as ">10." In analogy to the adhesion rate there is "another" bond formation rate that refers to all detectable single bonds of all force curves of the whole set of measurements.

With a leukocyte (Jurkat) on the cantilever, Moy et al. thoroughly investigated the interaction between the integrin LFA-1 ($\alpha_1\beta_2$) and a cell adhesion molecule ICAM-1 or ICAM-2 on a substrate (Wojcikiewicz et al., 2006).

In this intense study a large number of data were collected at 25°C (room temperature) to analyze the binding potentials of the integrin–I-CAM complexes with the Bell–Evans model at different loading rates (determined by the slope prior to the de-adhesion event). The recalculation from the measured most probable de-adhesion forces into the characteristics of the bond potential ΔG, Δx, and the off-rates matches very well to the picture of a receptor–ligand interaction. Two affinity states of the integrin that can be switched artificially by replacing the Ca^{2+} ions in the binding pocket of the integrin by Mg^{2+} were resolved. The adhesion force, in the presence of the Mg^{2+} increased by 25 pN for the I-CAM-1 and by 10 pN for I-CAM-2 bonding to the Mg^{2+} activated integrin. The adhesion strength determined by the area under the force (dissipated de-adhesion energy) was used to quantify the adhesion strength. I-CAM-1 showed a stronger de-adhesion energy than ICAM-2. A stimulation by PMA to induce molecular clustering of the integrin resulted in a pronounced increase (fourfold for I-CAM-1 and threefold for I-CAM-2) of de-adhesion energy.

Another integrin VLA-4 ($\alpha_4\beta_1$) also present in this leukocyte cell specifically recognizes the vascular cell adhesion molecule V-CAM-1. By cell adhesion measurements, the specific interaction between the integrin ($\alpha_4\beta_1$) and the adhesion molecule V-CAM-1 immobilized on a substrate (50–100/μm²) was studied at short contact times of some milliseconds for two reasons (Schmitz et al., 2008). One reason was to resemble the natural situation for the leukocyte cell that has to react very fast to a signal on the surface to establish adhesion. The other was to study the initiation of this adhesion on the single molecule level but not after an acquisition of several adhesion molecules leading to strong forces.

This study did emphasize the anchorage of the integrin ($\alpha_4\beta_1$) in the cellular membrane. For this reason, the individual force distance traces (as shown in Figure 9.21) have been thoroughly analyzed.

The trained eye recognizes the typical signature of membrane tethers from these curves (in particular in curve 5 of Figure 9.21). By selecting such ideal tether curves, the viscoelastic parameters of the membrane could be characterized utilizing the Kelvin-model (Figure 9.14) and fitting it to the traces (Figure 9.20): $k_i = 0.26$ pN/nm, $k_t = 1.6$ fN/nm and $\eta = 6$ fNs/nm.

As all integrins, the $\alpha_4\beta_1$ integrin has an increased affinity too, if Ca^{2+} is replaced by Mg^{2+}. However, the most probable adhesion force did not significantly change (from 26 to 25 pN with Mg^{2+}). This is because the membrane tethers act like force clamps. At 3 μm/s pulling velocity and 37°C, the tethers pulled from the Jurkat cells keep the receptor ligand complex at the constant force of 26 pN. For thermodynamic reasons, the integrins in the presence of Ca^{2+} are stochastically distributed in low affinity and high affinity states. The replacement of Ca^{2+} by Mg^{2+} shifts

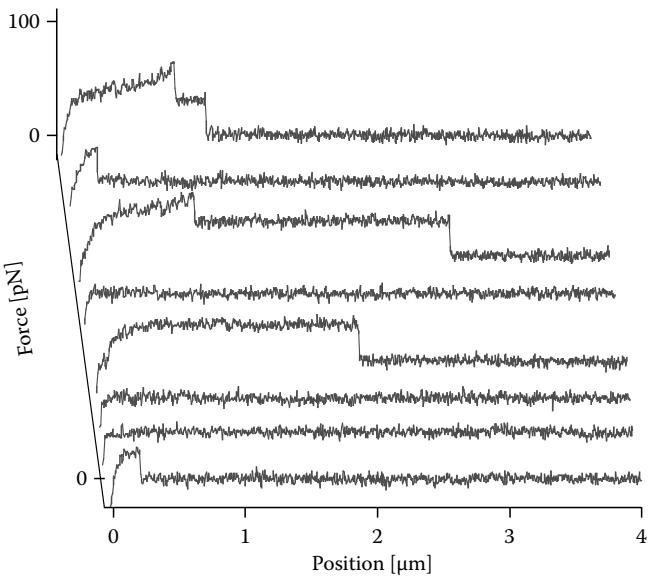

FIGURE 9.21 Subsequent force curves of Jurkat cells on a cantilever probed on a V-Cam-1-coated surface after contacts of 100 ms at 50 pN. Characteristic measures are the maximum force, the number of de-adhesion events per curve, the position and the step height of a de-adhesion event, or the area ("energy") spanned between the curve and the zero force line. The typical signature of a tether (the almost constant force plateau) ideally is represented in curve 5 (from above) in curve 3 is the longest tether a short one in the first curve overlaid by another adhesive feature. Curves 2 and 8 are too short to discern whether a tether was the origin of this trace. The curves 4, 6, and 7 are counted as non-adhesive events in the measure of the adhesion rate.

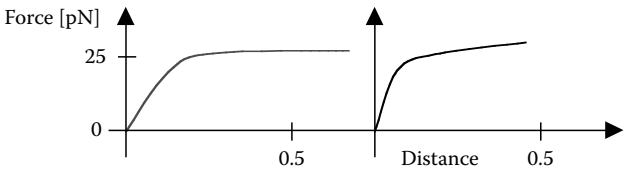

Substrate	Mg^{2+} and V-CAM-1	V-CAM-1
Tether rigidity k_t	0.9 fN/nm	1.6 fN/nm
Bending rigidity k_i	0.19 pN/nm	0.26 pN/nm
Tether length	700 nm	450 nm
De-adhesion force	25 pN	26 pN
Adhesion rate	39%	26%

FIGURE 9.22 Scheme of the "typical" force traces from force measurements between VLA-4 ($\alpha_4\beta_1$ integrin) and V-CAM-1, V-CAM-1 with Ca^{2+} replaced by Mg^{2+} (left). The differences in the force slopes are subtle: tethers are shorter, stiffer in the initial slope, and slightly steeper in the force plateau without Mg^{2+}.

this distribution toward a higher fraction of integrins with high affinity (Figure 9.22).

Nevertheless, the bond formation rate (fivefold), the adhesion rate, and the tether length significantly (twofold) are increased in the presence of Mg^{2+}. This indicates that the avidity of high affinity integrins has been increased. The viscous element η did not change. It remains unclear whether the tether length is increased, because Mg^{2+} alters the stiffness of the membrane or because the integrins are distributed into membrane areas of different stiffness. There is a likelihood that integrins in stiff areas (lipid rafts) show higher affinity in untreated cells. Adding Mg^{2+} activates all integrins including those in the soft areas.

Mg^{2+} artificially increases the affinity of an integrin, but the measured force does not indicate a stronger binding force. Here we clearly see how the cellular spacer dictates the measured, most probable, adhesion force by the tether plateau.* SDF-1 is a reporter for an inflammation in the tissue that is presented on the surface of blood vessel cells in the neighborhood of the inflammation. The chemokine SDF-1 is known to stimulate the G-protein-coupled CXCR-4 receptor of the Jurkat cells. The aim of the lymphocyte is to instantaneously react on that SDF-1 signal on the vascular endothelium with strong adhesion before the blood stream pushes it out of the region of inflammation. The tethering constantly slows down the lymphocyte, to allow for scrutinizing the vessel walls for SDF-1 molecules. The lymphocyte instantaneously stops and firmly adheres to subsequently leave the blood system for defeating the injury in the tissue.

In the age of nanotechnology, a very sophisticated experiment became possible. A non-adhesive surface was nano-patterned with hexagonally arranged adhesion spots at defined distances in the range of a few tens of nanometers. This nanofabricated surface was used to investigate the spatial requirements of receptor arrangements in molecular adhesion clusters (focal adhesion spots). The experiments revealed that cell adhesion, proliferation, and differentiation strongly depend on the nanoscale arrangement of adhesion ligands and in particular that the spacing between the single nanometer-sized adhesion spots is the key player for defining the cell's fate (Arnold et al., 2004). Adhesion force measurements show that such nanostructures influence cell adhesion strength and adhesion cluster formation during the first 5 min of adhesion itself (Selhuber-Unkel et al., 2008). Therefore, a cell immobilized on the cantilever stays in contact with such a nano-patterned adhesion surface with different spacings between adhesion sites for several seconds. While retracting the cell after the time of contact, from the force traces pronounced adhesion peaks up to some nN are identified. In Figure 9.23, the de-adhesion forces are summarized for the different spaced nano-patterns and contact times (Selhuber et al., 2006). By simultaneous fluorescence microscopy, these peaks were correlated to fluorescing focal adhesion sites on the substrate established by the cell at the time of contact (Selhuber-Unkel et al., submitted).

9.4.3.3 Spheres on Cells

Another example to defeat the cellular malfunction in the tissue is by the selective uptake of therapeutics in small vehicles by the targeted cells in an organism. This targeted uptake of specially designed vehicles, in particular, loaded with DNA by cells is a strong aim in medical research. The molecular composition of the external surface of such a vehicle shall determine the type of the target cell. In an adhesion force experiment, that mimics the small vehicle by a sphere of 5 µm radius immobilized to an AFM cantilever, the initial binding force of such a vehicle to a

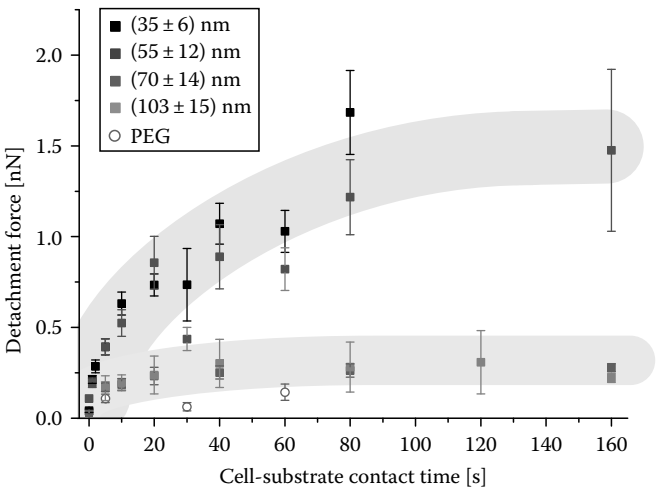

FIGURE 9.23 The critical spacing for the cooperative arrangement of adhesion molecules in focal contact is between 55 and 70 nm. Cell de-adhesion forces after contacts up to 160 min on substrates with different spaced adhesion sites (black and dark gray 55 nm and smaller; medium gray and light gray 70 nm and larger). Contacts on a plain PEG surface do not show significant adhesion. (From Selhuber-Unkel, C. et al., *Biophys. J.*, 98, 543, 2010. With permission.)

* The force might be even slightly decreased by the less rigid membrane environment of the majority of integrins.

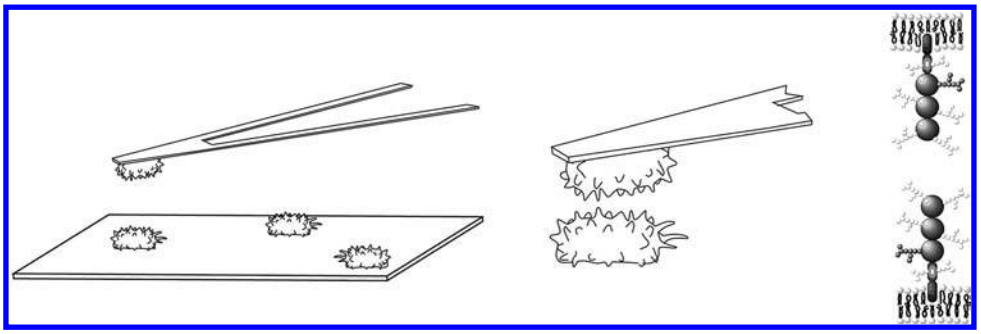

FIGURE 9.24 The *Dictyostelium* cell on the cantilever is brought in contact with another *Dictyostelium* cell as gently and short that only single csA molecules will interact with each other (hypothetical structure of a contact site A molecule on the right).

cell was quantified. Two different surfaces, positively (NH_2) and negatively (COOH) charged spheres, have been investigated on two different cell lines (MCF-10A and MDA-MB-4355) at 37°C in the nutrient medium (Munoz Javier et al., 2006). Since cells merely show a negative net charge by the sugar groups of the glycocalix, the results expectedly showed a higher adhesion rate of the positively charged spheres. The most probable "molecular"* adhesion force is increased from 20 pN (negative) to 25 pN for the positively charged spheres after a contact of 1 ms at 50 pN. Because of the increase in the adhesion rate from 20% (negative) to almost 80%, the net charge of the MCF-10A cell line appeared much more negatively charged than the MDA-MB-4355 cell line with a moderate increase from 30% (negative) to almost 50%.

9.4.3.4 Single Cell-to-Cell Measurements

Dictyostelium is a single cell organism (amoeba), which has been studied by bio-scientists for many years (Bozzaro et al., 2004; Jin and Hereld, 2006). It can change from a single cell organism into a multicellular organism (slug) by switching the active genes in the nucleus. For this purpose, *Dictyostelium* cells meet by the hot spot of a chemokine signal (cAMP) sent out from each switched cell. The switched cells start to produce a Ca^{2+} independent adhesion molecule csA (contact site A) in the extracellular membrane. In cell-to-cell adhesion measurements between *Dictyostelium discoideum* cells the adhesion force of the homophilic interaction between two individual csA molecules was to be investigated (Figure 9.24). This experiment now involves two unknown spacers into the force measurement. Luckily, the cells approximately behave identically and the sets of adhesion molecules in the cell membrane are known. Nevertheless, how is it possible to discern from the force signal, which pair of adhesion molecules from the orchestra of integrins and other adhesion molecules present on these cells interacts? *Dictyostelium* is a robust organism that even stands the removal of environmental Ca^{2+} for some hours. As we know, Ca^{2+} and Mg^{2+} are essential divalent anions to mediate the integrin adhesion. Luckily, all integrins and adhesion molecules of the *Dictyostelium* refuse to contribute to the adhesion measurements after the removal of these anions. The adhesion rate dropped to 3% (nonspecific interaction) after contacts of 0.1 s at 50 pN. By the adhesion force measurement without divalent anions, a most probable de-adhesion force between 20 and 23 pN was detected for the homophilic interaction between individual csA molecules at loading rates between 3 and 9 pN/s. After prolonged contacts—1 and 2 s—the force histograms showed pronounced force peaks at multiples of 23 pN (Benoit et al., 2000).

The csA molecule is known to be anchored solely in the external lipid layer of the membrane (ceramide anchor). A genetically modified mutant of *Dictyostelium* with a transmembrane anchor was used to test whether the bond between two csA molecules brakes or whether the molecule is extracted from the lipid bilayer. Since the force measurements showed no significant change between the two species the anchor is believed to be at least as strong as the molecular interaction and thus the csA is extracted from the membrane in less than 50% of the adhesion events (Benoit et al., 2000).

In a very challenging study (Panorchan et al., 2006a,b), the homophilic interaction forces between individual cadherin molecules (VE-, N- and E-cadherin) were measured (Figure 9.25). Despite the fact that the measurements have been performed between living cells, the force traces in this study do not show tethers but instead show WLC-like load to the bond. On the one hand, probably due to the strong spreading of the cells on the substrate, they might prevent tether formation by a high membrane tension. On the other hand, the cadherins (the E-cadherin in particular) might well be connected to the cytoskeleton by catenin complexes. By applying the Bell–Evans formalism, even an inner barrier of the E-cadherins' potential landscape was identified. The weakest de-adhesion forces were found in N-cadherin 17–30 pN, followed by the VE-cadherin interaction between 32 and 50 pN, and finally E-cadherin de-adhesion forces between 29 and 73 pN were measured at loading rates between 50 and 5000 pN/s.

9.4.3.5 Cell Layer-to-Surface Measurements

The presented examples of cell-adhesion force measurements aimed to measure initial adhesion or fast molecular processes at the level of single molecules. These measurements are important and they are practical. In contrast, long-term adhesion processes

* There is no statement on which molecules are responsible for the positive or the negative adhesion.

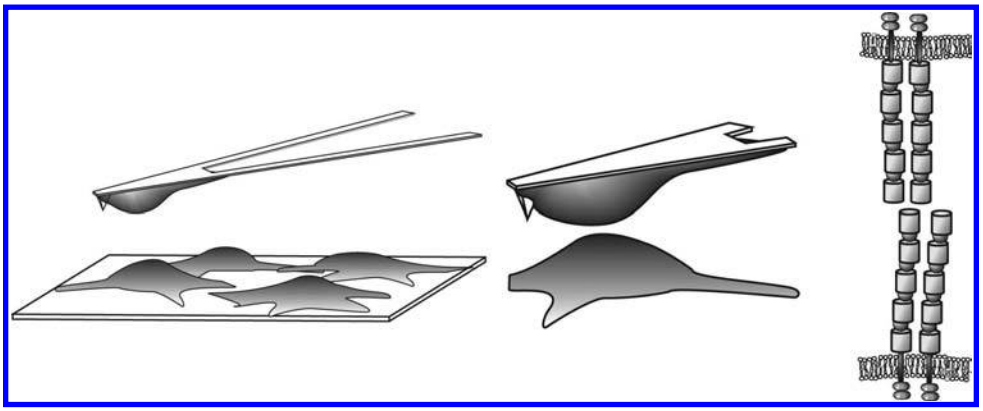

FIGURE 9.25 The homophilic interaction between individual cadherin dimers was measured by call adhesion force spectroscopy between HUVEC cells strongly adhering to the substrate and the cantilever. Schematics of the experiment and of the interacting cadherin dimers.

are difficult to measure in a force experiment. Cells that seem to like a surface for the first few seconds might decide to push it away after having explored it for an hour. How will the adhesion forces involved in the artificial bones and implants develop? With a bone cell layer on a cantilever potential, implant surfaces were probed to find out the durablilty, for the acceptance of implants by the adhering cells (Benoit and Gaub, 2002). The cell-to-surface contacts can be prolonged to several minutes, maybe up to an hour, but then the drift becomes a limiting factor and, force spectroscopy is not applicable for this purpose.

Another step into understanding the complexity of the cell adhesion experiments is made by the force measurements with cell layers. The number of cells interacting with the surface is unknown and the adhesion molecules contributing in parallel to the force trace are high. A typical force graph of a fibronectin-coated sphere mounted to the cantilever after a contact of 20 min at 5 nN on a layer of confluent RL cells is shown in Figure 9.26. After the contact, an approximated Hookean stretching of the cell layer (left arrow) takes place until by an increasing number of dissociating bonds and the progressed disentangling of membrane and cytoskeleton the maximum force is reached. The measured maximum adhesion forces are up to three orders of magnitudes higher than in a single molecule experiment. The large maximum adhesion force of 20 nN is the sum of several hundred or thousands of single molecules each contributing with their weak adhesion forces. Some of these contributing molecules

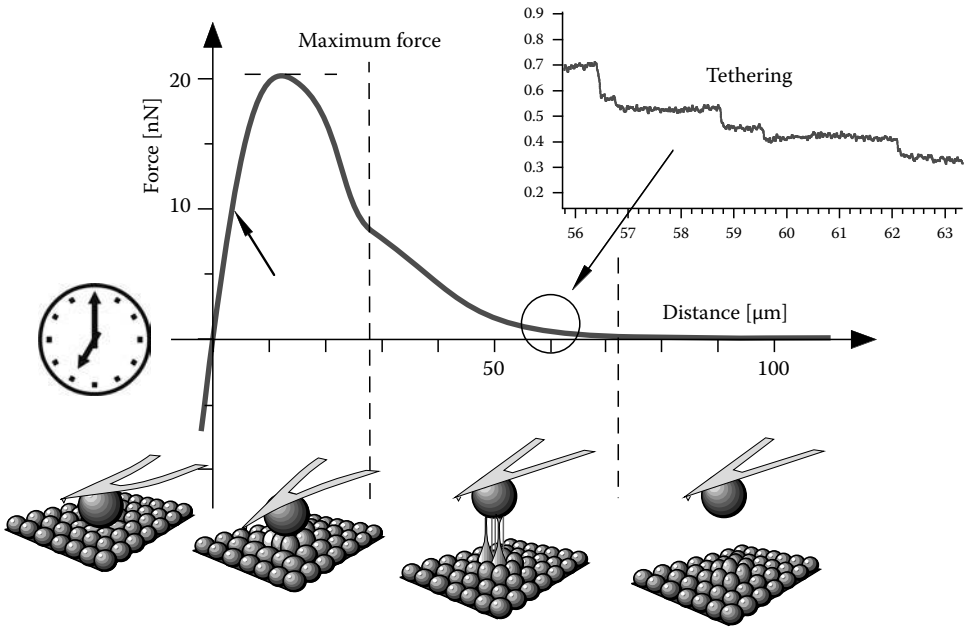

FIGURE 9.26 A typical force graph from an adhesion experiment between a fibronectin-functionalized sphere on a cell layer of JAR cells after a 20 min contact at 5 nN. The steep initial increase of the force reflects the predominantly elastic stretching of the participating cells. The individual unbinding events are not resolved in the scaling of this figure. Zooming in the descending shoulder of the tethering region unravels de-adhesion steps of individual membrane tethers. The scheme below the force trace illustrates the situation of the cells in the force experiment.

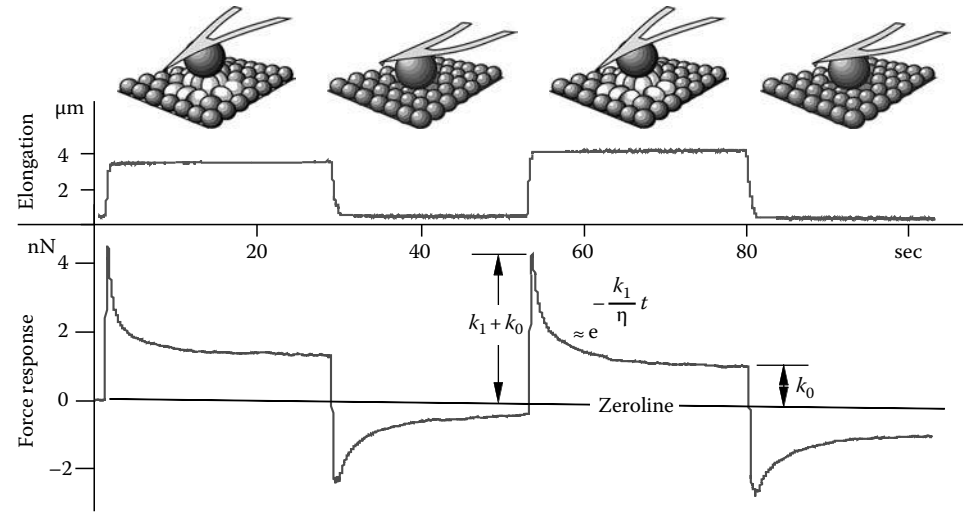

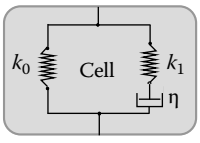

Cell line	k_0	k_1	η	Compliance
JAR	0.7 ± 0.2	2.1 ± 0.4	25 ± 7	(Intermediate)
HEC	0.4 ± 0.1	1 ± 0.3	4.9 ± 2.3	(Compliant)
RL	5.3 ± 0.2	3.5 ± 0.5	27 ± 9	(Rigid)
	pN/nm	pN/nm	pN*s/nm	

FIGURE 9.27 Schematics of a viscoelastic force experiment on a cell layer of a JAR, HEC, or RL cell line. Below the rectangular elongation pattern with plateau steps of 25 s and the measured force response of the cell layer. After the step jump that elongates the two parallel springs of the Kelvin model the dashpot relaxes logarithmically until k_1 is relaxed and k_0 keeps the tension constant. (Modified from Benoit, M. and Gaub, H.E., *Cells Tissues Organs*, 172, 174, 2002.)

are still resolved as individual de-adhesion events when zooming into the tethering region in the force traces' descending shoulder. An adhesive interaction length of several tens of micrometers is rarely seen in single molecule force measurements.

Such a configuration is perfectly suited to investigate the viscoelastic properties of a cell layer probed by a force load following a rectangular step function. With the fibronectin functionalized sphere the load can be indenting or pulling (Figure 9.27). If the force steps stay far below the maximum adhesion force the transition to the tethering region will not be reached within the duration of the force plateau until the back step. A typical force trace is represented in Figure 9.27. Modeling the cell layer with the Kelvin model, the force response is reproduced. The values of $k_1(=k_i)$, $k_0(=k_t)$, and η (=η) were determined from the force step experiment for different cell lines as listed in Figure 9.27.

Compared to a single tether the values of μ1, μ0, and η1 are larger by orders of magnitudes.

9.4.3.6 Cell Layers on Cell Layers

The highest level of complexity is reached by experiments between two cell layers. The surface geometry of the two cell layers is not defined already and can roughly be estimated by the indentation force, the radius of the sphere, and the elasticity of the interacting cells. The viscoelastic behavior of the two interacting cell layers can only be estimated from additional experiments (e.g., Figure 9.27). The advantages of this experimental design are that the cells can polarize, establish intercellular communication and other epithelial cell habits close to their natural behavior. The typical cluster of adhesion molecules as in tight junctions, gap junctions, or focal adhesions are established within the confluent cell layers. While the two cell layers are brought into contact, they might start to communicate and establish complex adhesion patterns (Pierres et al., 2007). Thousands of adhesion molecules and receptors are contributing to the measured de-adhesion forces in the range of several nN. The organization of a strong molecular adhesion cluster is known to last several minutes (Kawakami et al., 2001). Recognition, signaling, transport, and diffusion processes determine the time of the molecular composition at the adjacent cell membranes.

With fluorescence microscopy, molecular arrangements in focal adhesion spots can be visualized. Electron micrographs resolve these multi-molecular adhesion structures in fixed cells. The direct correlation of these images to the force is complemented by measurements (Selhuber et al., 2006) and theory (Schwarz et al., 2006). The following cell adhesion measurements between cell layers were conducted after contact times of up to 40 min at contact forces of 5 nN* and separation velocities of up to 7 μm/s (Thie et al., 1998).

* This relatively high force is necessary to ensure a stable cell contact for such a long time despite the drift effects.

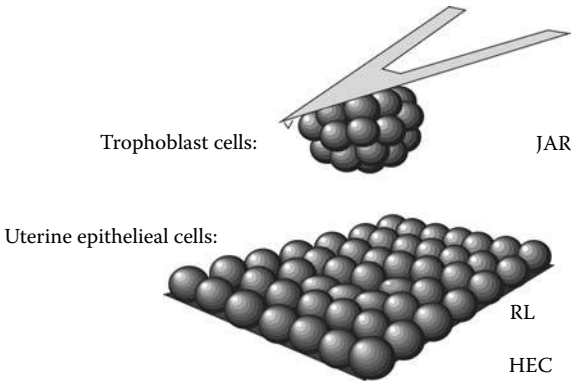

FIGURE 9.28 The JAR-cell line grown to fluency on the cantilever is brought into contact with either the confluent cell layer of RL cells or HEC cells for several minutes. The RL cell layer is known to firmly arrest the JAR sphere, whereas the HEC cell layer does not.

These pioneering force measurements from the last century are the first AFM adhesion force investigations involving living cell layers. The experimental setup comes as close as possible to the native situation in the human body: JAR-cells from a trophoblast cell line, grown on a sphere resembling the natural trophoblast structure in size, shape, and cellular arrangement of the apical region. RL95-2 cells or HEC-1-A cells, from uterine cell lines cultured in a petri dish resemble the uterine epithelial layer. Both cell layers where held in contact for several minutes at 5 nN with the trophoblast cell layer on the sphere until separation (as shown in Figure 9.28).

How long would it take to firmly arrest the trophoblast layer on either cell layer? Comparing the shorter contacts of 1 or 10 min to HEC or RL cell layers indicates a stronger adhesion to the HEC cells with respect to the maximum adhesion forces. Regarding the area under the curve representing the dissipated adhesion energy, after 10 min an enhanced energy dissipation is present for contacts between the RL and the JAR cell layers. After 20 min, the RL cells firmly connect their adhesion molecules into clusters that are strongly connected with the cytoskeleton in the complex interplay with the JAR cell layer. This was not evident from the maximum adhesion force, but by the adhesion pattern recorded while retracting the cellular trophoblast sphere on the AFM cantilever (see Figure 9.29) from the RL-cell layer and the HEC-cell layer, respectively. The adhesion strength can be quantified by the dissipated adhesion energy (area spanned by the force trace). In a view through the light microscope, after such a strong de-adhesion event at least one of the cell layers appeared to be severely damaged.

This crude method of investigating cellular adhesion is a relatively small step toward the origin of life and birth. These experiments about the homing of the dividing embryonic cells inside

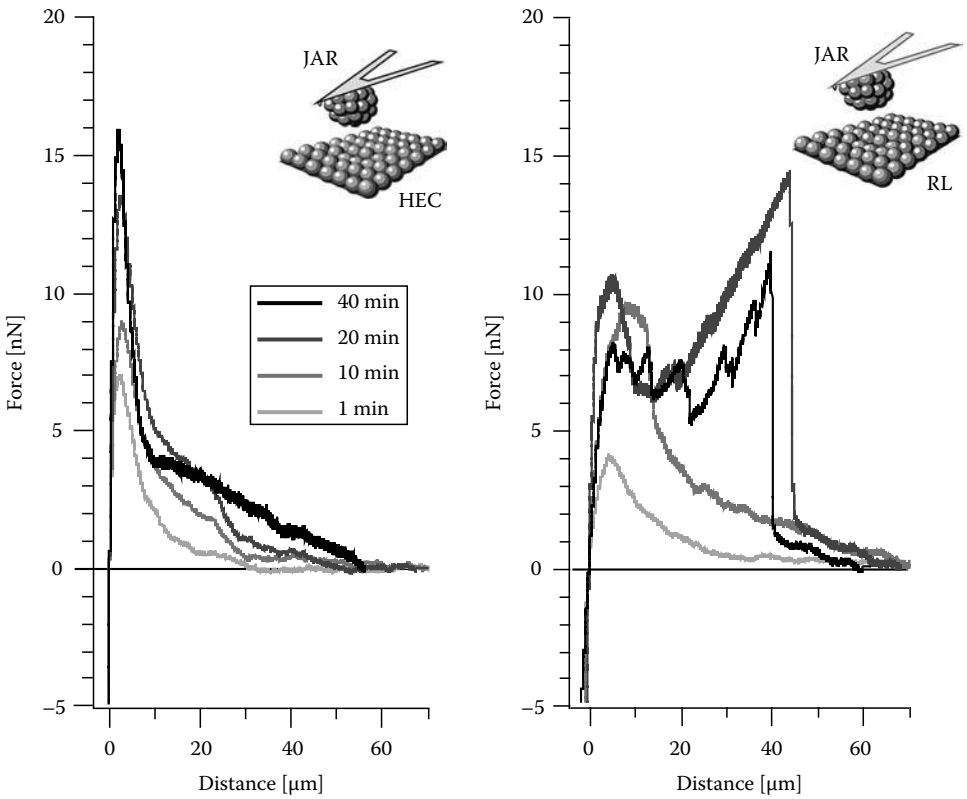

FIGURE 9.29 Typical sets of force traces with increased contact time from 1 to 40 min. Traces from the adhesion force measurements between a trophoblast cell layer (JAR) and a endometrium cell layer (HEC) on the left side, traces between a trophoblast cell layer and another endometrium cell layer (RL) on the right. (Modified from Thie, M. et al., *Hum. Reprod.*, 13, 3211, 1998.)

the trophoblast sphere in the female uterus show how tiny the steps of science are and how complex the mystery of life might be. On the other hand, this crude method neglects all the single molecules in the process in order to quantify a general phenomenon of cell adhesion, that is, molecular clustering. A zoom into the descending shoulders of the force traces allows for the counting of each single tether and measuring its step height that pools at 75 ± 15 pN.

The descending shoulders of the force curves, at higher force resolution, again uncover the individual detachment events of single integrins on membrane tethers (see Figure 9.26). Whether this adhesion pattern is a feature of the integrins $\alpha_4\beta_1$ and $\alpha_4\beta_6$ forming desmosomal structures and focal adhesion spots (Kawakami et al., 2001) or interactions contributed by other adhesion molecules remains a question.

Two general adhesion concepts appear from the experiment:

- The pealing off between the two cell layers, molecule by molecule, tether by tether, in analogy to one by one base pair in the DNA zipper configuration.
- The equally distributed force to many weak molecules in parallel as in the DNA in shear geometry.

Here the molecular clustering sums up a pronounced de-adhesion rupture event of 15 nN. From the force measurements of single integrins ($\alpha_4\beta_1$) a typical force appears to be between 20 and 60 pN at loading rates of 10–100 pN/s. Approximately 100–1000 molecular integrin bonds contribute to the measured clusters. They all have to be connected to the cytoskeleton, otherwise the cluster would separate from the cell forming a tether that we know will finally break at a force of about 300 pN since such a strong cluster of molecules would not release the tether again.

9.5 Conclusions

Experimentalists can directly measure mechanical properties of cells, cell layers and cellular membrane by force spectroscopy. Based on the parameters extracted from these measurements the complexity of the cell is described approximately by simplified viscoelasticity models. This is important for understanding cellular functions and the role of the cell in the background of the adhesion signal in an adhesion force measurement. The cell has a passive contribution as a spacer and as an agent for embedding the adhesion molecule, and it plays an active role when tuning the adhesion molecule or its molecular anchor. On a longer timescale, the formation of adhesion clusters is an important contribution of the active cell. From the incomplete collection of adhesion force experiments with the atomic force microscope ranging from single molecules to multi-molecular adhesion clusters, basic adhesion strategies of cells are unscrambled from the presented examples of force traces.

The application of the loading rate concept by Bell and Evans, that was developed to mechanically determine the adhesion strength of receptor–ligand interactions, has to be adapted to the mechanical properties of the cell, if possible. The membrane tether is of particular interest in this context for two reasons. It probes the adhesion complex in a force clamp at constant force and small loading rate on the one hand; on the other hand, the force trace contains subtle information about the membrane embedding of the adhesion molecule. So far, the molecular interactions have been studied from the chemical and thermodynamical point of view. Indeed, the molecular interactions of biomolecules on the scale of nanometers are mechanistic. These molecules are little machines and mechanical tools, plugs, and suspensions that can be described by classical mechanics. The cell-adhesion force measurements allow for this aspect and strongly contribute to the understanding of intracellular processes. Cell-adhesion force measurements even enable direct label free access to intracellular processes that imply changes in adhesion or viscoelastic behavior. For this reason, force measurements on the single molecular level gain interest not only for nano-bio-physics but also for molecular biology and medical sciences.

While classical physics aims to find "laws" that are valid for as many classes as possible, biology classically specifies the differences between classes, subclasses, and individuals of subclasses even down to the base pairs of their DNA. Physicists say: "a cell…" while biologists say, "we took an endothelial cell from the upper third of the dorsal endometrium in the early S2-phase of a 12 days old male…" For a cell-adhesion measurement with molecular resolution, the biophysicist has a dilemma. The information from the individual adhesion molecule is embedded in the concert of all the participating molecules of the cell including the membrane and the cytoskeleton. It is impossible to distinguish the contribution of each of them from the measured force signal.* The individual behavior of the investigated cell not only distorts a measured force trace, but furthermore it may not be determinable from which adhesion molecule a detected force signal originated from, because there are many classes of adhesion molecules, in different affinity states, present on the cellular surface.

With the knowledge of the typical adhesion patterns presented here, even complex force traces can be analyzed if a known signature of a certain molecule or a typical multi-molecular arrangement is identified in the trace. In some cases, the contribution of certain adhesion molecules can be ruled out just by luck or smart experimental design, by exclusion, blocking experiments, or by genetic knock out manipulation and silencing of a cell line. Subtracting the identified contributions of the "unwanted" molecules from measured force distributions often enhances the specific signal. Cells are organized to manage environmental strokes and often induce new uncertainties through unforeseen reactions, while the scientist tries to exclude molecules from the force experiment. Cells often have a back up for an eliminated molecule. Therefore, adhesion force experiments, conducted by

* Nuclear physicists have built enormous detectors to measure almost each particle from a collision experiment of just two elemental particles. Will biophysicists have to build similar detectors to measure the adhesion of just two cells?

an interdisciplinary team with members from chemical, medical, biological, and physical sciences benefit from the merge of knowledge, scientific strategies, and points of view to adequately reflect the complexity of each individual cell.

9.6 Outlook

Planar patch clamp technology turned out to be not only a perfect platform for AFM measurements on non-adherent cells, but also an extension toward simultaneous electrophysiological measurements, an application that is extremely attractive for pharmacological research. Here, for example, the mechanical signal from the cell can be correlated in time with the activity of membrane pores (Pamir et al., 2008).

Force spectroscopy not only characterizes antibodies with respect to their interaction force with their specific ligand, but also might identify diseases that are caused by the malfunction of cellular adhesion and optimize related medication.

Force measurements with the AFM sequentially measure, one interaction after the other at high resolution in force and space in a very time-consuming manner. A recent concept, that still has a high resolution in force but measures billions of interactions within a few seconds is the molecular force balance (Blank et al., 2004; Albrecht et al., 2008). This force balance might be a potential technique for high throughput force measurements on cells in the near future.

Acknowledgement

Many thanks to Prof. Dr. Hermann Gaub, for his great support and powerful lab space.

Abbreviations

A	Adenine (DNA base pair of thymine)
AFM	Atomic force microscope (sometimes, scanning force microscope SFM)
BR	Bacteriorhodopsin (optical driven proton pump of *H. salinaris*)
BFS	Bio-force sensor (red blood cell utilized as force sensor in a pipette)
BS-transition	Transition from the naturally B-formed DNA to the S-formed (S = stretched)
BSA	Bovine serum albumin
cAMP	Cyclic adenosine mono phosphate (chemokine)
C	Cytosine (DNA base pair of guanine)
csA	Contact site A
Ca^{2+}	Calcium divalent cation
CeNS	Center of Nano Science
CXCR	Receptor for cytosines of the CXC family (CXCR-4 is specific for SDF-1)
DNA	Deoxyribonucleic acid
E	Young's modulus (elastic modulus)
E-cadherin	Epithelial cadherin (cell adhesion molecule)
E. coli	*Escherichia coli* (bacterium)
EM	Electron microscope (SEM, scanning electron microscope)
FJC	Freely jointed chain (polymer model)
FRC	Freely rotating chain (polymer model)
G	Guanine (DNA base pair of cytosine)
GFP	Green fluorescent protein
HEC-1-A	Human uterine epithelial cell line
I-CAM	Inter cellular adhesion molecule
JAR	Human trophoblast-like cell line
K_D	Dissociation constant
k_B	Boltzmann constant
k_{off}	Unbinding rate
k_BT	Thermal energy equivalent of two degrees of freedom at a certain temperature
MCF-10A	Human mammary gland epithelial cell line
MD (MDS)	Molecular dynamics simulation
MDA-MB-4355	Human mammary gland epithelial cell line
Mg^{2+}	Magnesium divalent cation
MLCT	Description of industrial cantilevers (micro lever for contact and tapping mode)
N-cadherin	Neuronal cadherin (cell adhesion molecule)
nm	Nano meter
OT	Optical trap or optical tweezers (trapped bead in a laser focus as force sensor)
PAP-G	Last unit of the P-pilus consisting of several PAP-units that binds to galabiose
PN	Pico Newton
PMA	Parametoxyamphetamine (influences intracellular cell signaling)
RGD	(*Arg*inin-*Gly*cin-*Asp*aragin) integrin specific peptide sequence
RL95-2	Human uterine epithelial cell line
SDF-1	Stromal derived factor-1
Si	Silicon
SiO	Silicon oxide
SiN	Silicon nitride
T	Thymine (DNA Base pair of adenine)
V-CAM	Vascular cell adhesion molecule
VE-cadherin	Vascular endothelial cadherin (cell adhesion molecule)
VLA-4	Very late antigen-4
WLC	Worm-like chain (polymer model)
ΔG	Gibbs free energy
ν	Poisson ratio (compressibility)

References

Alberts, B., Johnson, A., Lewis, J., Raff, M., Roberts, K., and Walter, P. (2002) *Molecular Biology of the Cell*, Garland Science, New York.

Albrecht, C. H., Neuert, G., Lugmaier, R. A., and Gaub, H. E. (2008) Molecular force balance measurements reveal that dsDNA unbinds under force in rate dependent pathways. *Biophys J*, 94, 4766–4774.

Arnold, M., Cavalcanti-Adam, E. A., Glass, R., Blummel, J., Eck, W., Kantlehner, M., Kessler, H., and Spatz, J. P. (2004) Activation of integrin function by nanopatterned adhesive interfaces. *Chemphyschem*, 5, 383–388.

Bell, G. I. (1978) Models for the specific adhesion of cells to cells. *Science*, 200, 618–627.

Benoit, M. (2002) Cell adhesion measured by force spectroscopy on living cells. *Methods Cell Biol*, 68, 91–114.

Benoit, M. and Gaub, H. E. (2002) Measuring cell adhesion forces with the atomic force microscope at the molecular level. *Cells Tissues Organs*, 172, 174–189.

Benoit, M., Gabriel, D., Gerisch, G., and Gaub, H. E. (2000) Discrete interactions in cell adhesion measured by single-molecule force spectroscopy. *Nat Cell Biol*, 2, 313–317.

Besser, A. and Safran, S. A. (2006) Force-induced adsorption and anisotropic growth of focal adhesions. *Biophys J*, 90, 3469–3484.

Binnig, G., Quate, C. F., and Gerber, C. (1986) Atomic force microscope. *Phys Rev Lett*, 56, 930–933.

Blank, K., Lankenau, A., Mai, T., Schiffmann, S., Gilbert, I., Hirler, S., Albrecht, C., Benoit, M., Gaub, H. E., and Clausen-Schaumann, H. (2004) Double-chip protein arrays: Force-based multiplex sandwich immunoassays with increased specificity. *Anal Bioanal Chem*, 379, 974–981.

Bozzaro, S., Fisher, P. R., Loomis, W., Satir, P., and Segall, J. E. (2004) Guenther Gerisch and *Dictyostelium*, the microbial model for ameboid motility and multicellular morphogenesis. *Trends Cell Biol*, 14, 585–588.

Butt, H.-J. R., Cappella, B., and Kappl, M. (2005) Force measurements with the atomic force microscope: Technique, interpretation and applications. *Surf Sci Rep*, 59, 1.

Carrion-Vazquez, M., Oberhauser, A. F., Fisher, T. E., Marszalek, P. E., Li, H., and Fernandez, J. M. (2000) Mechanical design of proteins studied by single-molecule force spectroscopy and protein engineering. *Prog Biophys Mol Biol*, 74, 63–91.

Clausen-Schaumann, H., Seitz, M., Krautbauer, R., and Gaub, H. E. (2000) Force spectroscopy with single bio-molecules. *Curr Opin Chem Biol*, 4, 524–530.

Collin, D., Ritort, F., Jarzynski, C., Smith, S. B., Tinoco, I. Jr., and Bustamante, C. (2005) Verification of the Crooks fluctuation theorem and recovery of RNA folding free energies. *Nature*, 437, 231–234.

Dettmann, W., Grandbois, M., Andre, S., Benoit, M., Wehle, A. K., Kaltner, H., Gabius, H. J., and Gaub, H. E. (2000) Differences in zero-force and force-driven kinetics of ligand dissociation from beta-galactoside-specific proteins (plant and animal lectins, immunoglobulin G) monitored by plasmon resonance and dynamic single molecule force microscopy. *Arch Biochem Biophys*, 383, 157–170.

Dewa, T., Sugiura, R., Suemori, Y., Sugimoto, M., Takeuchi, T., Hiro, A., Iida, K., Gardiner, A. T., Cogdell, R. J., and Nango, M. (2006) Lateral organization of a membrane protein in a supported binary lipid domain: Direct observation of the organization of bacterial light-harvesting complex 2 by total internal reflection fluorescence microscopy. *Langmuir*, 22, 5412–5418.

Dietz, H. and Rief, M. (2004) Exploring the energy landscape of GFP by single-molecule mechanical experiments. *Proc Natl Acad Sci USA*, 101, 16192–16197.

Dietz, H. and Rief, M. (2006) Protein structure by mechanical triangulation. *Proc Natl Acad Sci USA*, 103, 1244–1247.

Discher, D. E., Boal, D. H., and Boey, S. K. (1998) Simulations of the erythrocyte cytoskeleton at large deformation. II. Micropipette aspiration. *Biophys J*, 75, 1584–1597.

Erdmann, T. and Schwarz, U. S. (2006) Bistability of cell-matrix adhesions resulting from nonlinear receptor–ligand dynamics. *Biophys J*, 91, L60–L62.

Evans, E. (1998) Energy landscapes of biomolecular adhesion and receptor anchoring at interfaces explored with dynamic force spectroscopy. *Faraday Discuss*, 111, 1–16.

Evans, E., Heinrich, V., Ludwig, F., and Rawicz, W. (2003) Dynamic tension spectroscopy and strength of biomembranes. *Biophys J*, 85, 2342–2350.

Florin, E. L., Moy, V. T., and Gaub, H. E. (1994) Adhesion forces between individual ligand-receptor pairs. *Science*, 264, 415–417.

Franz, C. M., Taubenberger, A., Puech, P. H., and Muller, D. J. (2007) Studying integrin-mediated cell adhesion at the single-molecule level using AFM force spectroscopy. *Sci Stke*, 2007, l5.

Fung, Y. C. (1993) *Biomechanics—Mechanical Properties of Living Tissues*, Springer, New York.

Godin, M., Bryan, A. K., Burg, T., Babcock, K., and Manalis, S. R. (2007) Measuring the mass, density and size of particles and cells using a suspended microchannel resonator. *Appl Phys Lett*, 91, 123121.

Grandbois, M., Beyer, M., Rief, M., Clausen-Schaumann, H., and Gaub, H. E. (1999) How strong is a covalent bond? *Science*, 283, 1727–1730.

Grandbois, M., Dettmann, W., Benoit, M., and Gaub, H. E. (2000) Affinity imaging of red blood cells using an atomic force microscope. *J Histochem Cytochem*, 48, 719–724.

Grubmuller, H., Heymann, B., and Tavan, P. (1996) Ligand binding: Molecular mechanics calculation of the streptavidin-biotin rupture force. *Science*, 271, 997–999.

Hansma, P. K., Elings, V. B., Marti, O., and Bracker, C. E. (1988) Scanning tunneling microscopy and atomic force microscopy: Application to biology and technology. *Science*, 242, 209–216.

Harmandaris, V. A. and Deserno, M. (2006) A novel method for measuring the bending rigidity of model lipid membranes by simulating tethers. *J Chem Phys*, 125, 204905.

Heimburg, T. (2007) Front matter. *Thermal Biophysics of Membranes.*

Helenius, J., Heisenberg, C. P., Gaub, H. E., and Muller, D. J. (2008) Single-cell force spectroscopy. *J Cell Sci*, 121, 1785–1791.

Hertz, H. (1882) Über die Berührung fester elastischer Körper. *Reine Angewandte Mathematik*, 92, 156–171.

Hochmuth, F. M., Shao, J. Y., Dai, J., and Sheetz, M. P. (1996) Deformation and flow of membrane into tethers extracted from neuronal growth cones. *Biophys J*, 70, 358–369.

Hugel, T., Rief, M., Seitz, M., Gaub, H. E., and Netz, R. R. (2005) Highly stretched single polymers: Atomic-force-microscope experiments versus ab-initio theory. *Phys Rev Lett*, 94, 048301.

Hwang, W. C. and Waugh, R. E. (1997) Energy of dissociation of lipid bilayer from the membrane skeleton of red blood cells. *Biophys J*, 72, 2669–2678.

Isralewitz, B., Gao, M., and Schulten, K. (2001) Steered molecular dynamics and mechanical functions of proteins. *Curr Opin Struct Biol*, 11, 224–230.

Jin, T. and Hereld, D. (2006) Moving toward understanding eukaryotic chemotaxis. *Eur J Cell Biol*, 85, 905–913.

Kawakami, K., Tatsumi, H., and Sokabe, M. (2001) Dynamics of integrin clustering at focal contacts of endothelial cells studied by multimode imaging microscopy. *J Cell Sci*, 114, 3125–3135.

Kruithof, M., Chien, F., de Jager, M., and van Noort, J. (2008) Subpiconewton dynamic force spectroscopy using magnetic tweezers. *Biophys J*, 94, 2343–2348.

Kufer, S. K., Dietz, H., Albrecht, C., Blank, K., Kardinal, A., Rief, M., and Gaub, H. E. (2005) Covalent immobilization of recombinant fusion proteins with hAGT for single molecule force spectroscopy. *Eur Biophys J*, 35, 72–78.

Kufer, S. K., Puchner, E. M., Gumpp, H., Liedl, T., and Gaub, H. E. (2008) Single-molecule cut-and-paste surface assembly. *Science*, 319, 594–596.

Lamontagne, C. A., Cuerrier, C. M., and Grandbois, M. (2008) AFM as a tool to probe and manipulate cellular processes. *Pflugers Arch*, 456, 61–70.

Ludwig, T., Kirmse, R., Poole, K., and Schwarz, U. S. (2008) Probing cellular microenvironments and tissue remodeling by atomic force microscopy. *Pflugers Arch*, 456, 29–49.

Lugmaier, R. A., Schedin, S., Kuhner, F., and Benoit, M. (2008) Dynamic restacking of *Escherichia coli* P-pili. *Eur Biophys J*, 37, 111–120.

Marcus, W. D. and Hochmuth, R. M. (2002) Experimental studies of membrane tethers formed from human neutrophils. *Ann Biomed Eng*, 30, 1273–1280.

Merkel, R., Nassoy, P., Leung, A., Ritchie, K., and Evans, E. (1999) Energy landscapes of receptor–ligand bonds explored with dynamic force spectroscopy. *Nature*, 397, 50–53.

Morfill, J., Blank, K., Zahnd, C., Luginbuhl, B., Kuhner, F., Gottschalk, K. E., Pluckthun, A., and Gaub, H. E. (2007) Affinity-matured recombinant antibody fragments analyzed by single-molecule force spectroscopy. *Biophys J*, 93, 3583–3590.

Muller, D. J., Kessler, M., Oesterhelt, F., Moller, C., Oesterhelt, D., and Gaub, H. (2002) Stability of bacteriorhodopsin alpha-helices and loops analyzed by single-molecule force spectroscopy. *Biophys J*, 83, 3578–3588.

Munoz Javier, A., Kreft, O., Piera Alberola, A., Kirchner, C., Zebli, B., Susha, A. S., Horn, E., Kempter, S., Skirtach, A. G., Rogach, A. L., Radler, J., Sukhorukov, G. B., Benoit, M., and Parak, W. J. (2006) Combined atomic force microscopy and optical microscopy measurements as a method to investigate particle uptake by cells. *Small*, 2, 394–400.

Oesterhelt, F., Oesterhelt, D., Pfeiffer, M., Engel, A., Gaub, H. E., and Muller, D. J. (2000) Unfolding pathways of individual bacteriorhodopsins. *Science*, 288, 143–146.

Pamir, E., George, M., Fertig, N., and Benoit, M. (2008) Planar patch-clamp force microscopy on living cells. *Ultramicroscopy*, 108, 552–557.

Panorchan, P., George, J. P., and Wirtz, D. (2006a) Probing intercellular interactions between vascular endothelial cadherin pairs at single-molecule resolution and in living cells. *J Mol Biol*, 358, 665–674.

Panorchan, P., Thompson, M. S., Davis, K. J., Tseng, Y., Konstantopoulos, K., and Wirtz, D. (2006b) Single-molecule analysis of cadherin-mediated cell-cell adhesion. *J Cell Sci*, 119, 66–74.

Parot, P., Dufrene, Y. F., Hinterdorfer, P., Le Grimellec, C., Navajas, D., Pellequer, J. L., and Scheuring, S. (2007) Past, present and future of atomic force microscopy in life sciences and medicine. *J Mol Recognit*, 20, 418–431.

Pierres, A., Prakasam, A., Touchard, D., Benoliel, A. M., Bongrand, P., and Leckband, D. (2007) Dissecting subsecond cadherin bound states reveals an efficient way for cells to achieve ultrafast probing of their environment. *FEBS Lett*, 581, 1841–1846.

Puchner, E. M., Alexandrovich, A., Kho, A. L., Hensen, U., Schafer, L. V., Brandmeier, B., Grater, F., Grubmuller, H., Gaub, H. E., and Gautel, M. (2008a) Mechanoenzymatics of titin kinase. *Proc Natl Acad Sci USA*, 105, 13385–13390.

Puchner, E. M., Franzen, G., Gautel, M., and Gaub, H. E. (2008b) Comparing proteins by their unfolding pattern. *Biophys J*, 95, 426–434.

Puech, P. H., Poole, K., Knebel, D., and Muller, D. J. (2006) A new technical approach to quantify cell-cell adhesion forces by AFM. *Ultramicroscopy*, 106, 637–644.

Radmacher, M. (2002) Measuring the elastic properties of living cells by the atomic force microscope. *Methods Cell Biol*, 68, 67–90.

Radmacher, M., Tillamnn, R. W., Fritz, M., and Gaub, H. E. (1992) From molecules to cells: Imaging soft samples with the atomic force microscope. *Science*, 257, 1900–1905.

Raucher, D. and Sheetz, M. P. (1999) Characteristics of a membrane reservoir buffering membrane tension. *Biophys J*, 77, 1992–2002.

Rico, F. and Moy, V. T. (2007) Energy landscape roughness of the streptavidin-biotin interaction. *J Mol Recognit*, 20, 495–501.

Rief, M., Clausen-Schaumann, H., and Gaub, H. E. (1999) Sequence-dependent mechanics of single DNA molecules. *Nat Struct Biol*, 6, 346–349.

Rief, M., Gautel, M., Oesterhelt, F., Fernandez, J. M., and Gaub, H. E. (1997a) Reversible unfolding of individual titin immunoglobulin domains by AFM. *Science*, 276, 1109–1112.

Rief, M., Oesterhelt, F., Heymann, B., and Gaub, H. E. (1997b) Single molecule force spectroscopy on polysaccharides by atomic force microscopy. *Science*, 275, 1295–1297.

Rief, M., Gautel, M., and Gaub, H. E. (2000a) Unfolding forces of titin and fibronectin domains directly measured by AFM. *Adv Exp Med Biol*, 481, 129–136; discussion 137–141.

Rief, M., Rock, R. S., Mehta, A. D., Mooseker, M. S., Cheney, R. E., and Spudich, J. A. (2000b) Myosin-V stepping kinetics: A molecular model for processivity. *Proc Natl Acad Sci USA*, 97, 9482–9486.

Ryu, W., Huang, Z., Sun Park, J., Moseley, J., Grossman, A. R., Fasching, R. J., and Prinz, F. B. (2008) Open micro-fluidic system for atomic force microscopy-guided in situ electrochemical probing of a single cell. *Lab Chip*, 8, 1460–1467.

Sackmann, E. (1995) Physical basis of self-organization and function of membranes: Physics of vesicles. In Lipowsky, R. and Sackmann, E. (Eds.) *Structure and Dynamics of Membranes*, Elsevier, Amsterdam, the Netherlands.

Schindler, H., Badt, D., Hinterdorfer, P., Kienberger, F., Raab, A., Wielert-Badt, S., and Pastushenko, V. (2000) Optimal sensitivity for molecular recognition MAC-mode AFM. *Ultramicroscopy*, 82, 227–235.

Schmitz, J. and Gottschalk, K. E. (2008) Mechanical regulation of cell adhesion. *Soft Matter*, 4(7), 1373–1387.

Schmitz, J., Benoit, M., and Gottschalk, K. E. (2008) The viscoelasticity of membrane tethers and its importance for cell adhesion. *Biophys J*, 95, 1448–1459.

Schwarz, U. S., Erdmann, T., and Bischofs, I. B. (2006) Focal adhesions as mechanosensors: The two-spring model. *Biosystems*, 83, 225–232.

Seifert, U. and Lipowsky, R. (1995) The morphology of vesicles. In Lipowsky, R. and Sackmann, E. (Eds.) *Structure and Dynamics of Membranes*, Elsevier, Amsterdam, the Netherlands.

Selhuber, C., Blummel, J., Czerwinski, F., and Spatz, J. P. (2006) Tuning surface energies with nanopatterned substrates. *Nano Lett*, 6, 267–270.

Selhuber-Unkel, C., Lopez-Garcia, M., Kessler, H., and Spatz, J. P. (2008) Cooperativity in adhesion cluster formation during initial cell adhesion. *Biophys J*, 95, 5424–5431.

Selhuber-Unkel, C., Erdmann, T., López-García, M., Kessler, H., Schwarz, U. S., and Spatz, J. P. (2010) Cell adhesion strength is controlled by intermolecular spacing of adhesion receptors. *Biophys J*, 98, 543–551.

Sens, P. and Turner, M. S. (2006) Budded membrane microdomains as tension regulators. *Phys Rev E Stat Nonlin Soft Matter Phys*, 73, 031918.

Sun, M., Graham, J. S., Hegedus, B., Marga, F., Zhang, Y., Forgacs, G., and Grandbois, M. (2005) Multiple membrane tethers probed by atomic force microscopy. *Biophys J*, 89, 4320–4329.

Thie, M., Rospel, R., Dettmann, W., Benoit, M., Ludwig, M., Gaub, H. E., and Denker, H. W. (1998) Interactions between trophoblast and uterine epithelium: Monitoring of adhesive forces. *Hum Reprod*, 13, 3211–3219.

Walton, E. B., Lee, S., and Van Vliet, K. J. (2008) Extending Bell's model: How force transducer stiffness alters measured unbinding forces and kinetics of molecular complexes. *Biophys J*, 94, 2621–2630.

Waugh, R. E. and Hochmuth, R. M. (1987) Mechanical equilibrium of thick, hollow, liquid membrane cylinders. *Biophys J*, 52, 391–400.

Wojcikiewicz, E. P., Zhang, X., and Moy, V. T. (2004) Force and compliance measurements on living cells using atomic force microscopy (AFM). *Biol Proc Online*, 6, 1–9.

Wojcikiewicz, E. P., Abdulreda, M. H., Zhang, X., and Moy, V. T. (2006) Force spectroscopy of LFA-1 and its ligands, ICAM-1 and ICAM-2. *Biomacromolecules*, 7, 3188–3195.